

**CONTINUOUS SCANNING LASER DOPPLER VIBROMETRY FOR
SYNCHRONIZED ARRAY MEASUREMENTS: APPLICATIONS TO
NON-CONTACT SENSING OF HUMAN BODY VIBRATIONS**

A Dissertation
Presented to
The Academic Faculty

by

Muhammad Salman

In Partial Fulfillment
of the Requirements for the Degree
Doctor of Philosophy in the
Woodruff School of Mechanical Engineering

Georgia Institute of Technology
December 2012

Copyright © 2012 by Muhammad Salman

**CONTINUOUS SCANNING LASER DOPPLER VIBROMETRY FOR
SYNCHRONIZED ARRAY MEASUREMENTS: APPLICATIONS TO
NON-CONTACT SENSING OF HUMAN BODY VIBRATIONS**

Approved by:

Dr. Karim Sabra, Advisor
Woodruff School of Mechanical
Engineering
Georgia Institute of Technology

Dr. François Guillot
Woodruff School of Mechanical
Engineering
Georgia Institute of Technology

Dr. Massimo Ruzzene
School of Aerospace Engineering
Georgia Institute of Technology

Dr. Minoru Shinohara
School of Applied Physiology
Georgia Institute of Technology

Dr. Yves H. Berthelot
Woodruff School of Mechanical
Engineering
Georgia Institute of Technology

Date Approved: Aug 20, 2012

DEDICATION

*To my parents, my wife and children,
elder brother and younger sister,
for their love, prayers and continued support
throughout my educational career*

ACKNOWLEDGEMENTS

I would like to thank my advisor, Dr. Karim Sabra for his politeness and willingness to guide me despite his busy schedule. He provided me great degree of freedom and flexibility in my research. Each time I visited his office, he welcomed me and provided the best solution to my research problems. I liked his new ideas to further steer my research projects to the right direction. He not only took care of the research problems but also provided the graduate assistantship. He developed my expertise of a team leader by providing me an opportunity to lead a team of senior design project which came in the list of top ten design projects.

I am very thankful to Dr. Yves H. Berthelot because of his generosity and continued support to let me use equipment from his research laboratory. His research lab had been a great source for setting up my experimental hardware related with optics such as lasers, lenses, shaker etc. I am very grateful to Dr. Minoru Shinohara for motivating me to implement new design techniques to measure the stiffness of human skeletal muscles and tendons. I would also like to acknowledge Dr. François Guillot for his humbleness and support to provide me his lecture notes about the LDV principle. I often asked him to proof read my ASA (Acoustical Society of America) presentations. My gratitude also goes to Dr. Massimo Ruzzene for providing me the knowledge about Structural Acoustics in his class which cleared important aspects of acoustics.

I acknowledge the teaching and guidance of all professors from whom I acquired valuable knowledge about Mechanical Engineering. I would like to mention some of the Professors' names (Georgia Institute of Technology) here for acknowledging their efforts to transfer useful knowledge, Dr. Karim Sabra, Dr. Wayne Whiteman, Dr. William Singhose, Dr. Harvey Lipkin, Dr. David Rosen, Dr. Charles Ume, Dr. Jonathan Colton, Dr. Shreyes Melkote, Dr. Steven Liang, Dr. Kyriaki Kalaitzidou, Dr. Levent Degertekin and Dr. Jun Ueda. I am also grateful to my research mates who gave me their valuable time, skills and

enthusiasm, during these years. My Ph.D. study at the Woodruff School of Mechanical Engineering has been a valuable learning experience.

Finally I would like to thank my parents, my wife and children, elder brother and younger sister, for their love, patience and prayers since the last six years especially, while I am far away from their eyes. I appreciate their patience and prayers without which my Ph.D. work would have been extremely difficult.

SUMMARY

Laser Doppler Vibrometry (LDV) is a non-contact technique for sensing surface vibrations. Traditionally, LDV uses one or more fixed beams to measure the vibrational velocity of specific points and orientations. In order to measure an angular velocity at least two laser beams are required. Instead, this research proposes to develop a Continuous Scanning Laser Doppler Vibrometer (CSLDV) technique, based on a single laser beam continuously sweeping the area of interest using a scanning mirror. Linear scans allow the measurement of normal and angular velocity while circular scans allow the measurement of normal velocity and two angular velocities. The first part of the study analyzes the performance of rigid body models of both the short line and circular scans (< 1 cm) for measuring low broadband frequency vibrations of gel samples. This thesis focused on low frequency broadband vibration since natural human body vibrations (such as tremor or breathing) are typically below a few hundred hertz. Results for normal and angular velocity measurements are validated against conventional method of using two fixed LDVs. The second part of this research investigates the CSLDV technique for longer scans (≥ 5 cm). These long scans will be used to act as an array of virtual transducers at multiple points along the scanning path of the single laser beam; thus yielding similar information obtained using an array of several real fixed LDVs. A practical challenge encountered when using CSLDV is speckle noise, that is generated when a coherent light source is reflected back from an optically rough surface. The effect of speckle noise will be quantified by varying different parameters such as scan lengths, scanning frequency, target to sensor distance and the amplitude of excitation. These parameters will be optimized in order to reduce the error of vibration measurements obtained from the CSLDV. Such systems will be used to monitor multiple degrees of freedom of human skeletal muscle vibrations for elastography purposes. The forced vibration of human muscles will be analyzed using these CSLDV techniques. Overall contributions of this work include: (1) Validation of rigid body models

of both short line and circular scans CSLDV for broadband low frequency linear and angular velocity measurements; (2) application to sensing natural human body vibrations (e.g., hand tremors); (3) replacement of an array of vibration sensors by a single long line scan CSLDV. (4) development of a dynamic elastography technique for skeletal muscles using CSLDV.

TABLE OF CONTENTS

DEDICATION	iii
ACKNOWLEDGEMENTS	iv
SUMMARY	vi
LIST OF TABLES	x
LIST OF FIGURES	xi
I INTRODUCTION	1
1.1 Introduction to laser Doppler vibrometer	1
1.1.1 Different methods of LDV sensing and their applications	1
1.1.2 Continuous Scanning LDV (CSLDV)	2
1.1.3 Types of CSLDV used in this research	4
1.2 Speckle noise	5
1.3 Benefits of CSLDV for bio-mechanical application	7
1.4 Elastic properties of skeletal muscles	7
1.5 Dynamic elastography	8
1.6 Motivation and objectives	9
1.7 Structure of thesis	11
II SHORT SCAN	13
2.1 Theory	14
2.1.1 Geometry for line and circular short scans	14
2.1.2 Data processing for broadband vibration	15
2.2 Experimental validation	17
2.2.1 Experimental setup	17
2.2.2 Experimental comparison between fixed LDV and the CSLDV	21
2.2.3 Sources of measurements errors	22
2.3 Applications to hand tremor sensing	28
2.4 Summary and conclusions	30

III LONG SCAN	32
3.1 Methodology: demultiplexing the CSLDV signal	32
3.2 Experimental validation	35
3.2.1 Experimental setup	35
3.2.2 Influence of speckle noise on the CSLDV signal	37
3.2.3 Comparison between fixed LDV and CSLDV measurements	39
3.2.4 Matched filtering of virtual sensors from CSLDV	39
3.3 Difference of phase velocities	43
3.4 Summary and conclusions	44
IV ELASTOGRAPHY	46
4.1 Dynamic elastography	46
4.2 Experimental setup	47
4.2.1 Design of the fixture for biceps contraction setup	47
4.2.2 Complete experimental setup	47
4.3 Application to dynamic elastography	50
4.3.1 Experimental protocol	50
4.3.2 Experimental results	51
4.3.3 Simple biomechanical model	52
4.3.4 Robustness of the CSLDV technique	53
4.3.5 Biceps contraction data for 10 subjects	54
4.3.6 Effect of wrist positions on the biceps stiffness	55
4.3.7 Sources of errors and limitations	57
4.4 Summary and conclusions	61
V CONCLUSIONS AND FUTURE WORK	63
5.1 Summary	63
5.2 Key Contributions	63
5.3 Recommendations for Future Research	64
APPENDIX A — LDV PRINCIPLE	67
APPENDIX B — SHORT SCAN	73
REFERENCES	75

LIST OF TABLES

1	Variation of error vs the distance, L for a circular scan of 10 mm diameter.	26
2	Data for neutral 90° elbow joint angle	58
3	R-Squared value for neutral 90° elbow joint angle	58
4	Data for supine 90° elbow joint angle	59
5	R-Squared value for supine 90° elbow joint angle	59
6	Data for neutral 120° elbow joint angle	60
7	R-Squared value for neutral 120° elbow joint angle	60
8	Data for neutral 150° elbow joint angle	61
9	R-Squared value for neutral 150° elbow joint angle	61

LIST OF FIGURES

1	Types of scans	3
2	Scan types used for this research	5
3	Speckle phenomena	5
4	Benefits of CSLDV for bio-mechanical application	7
5	Rigid body models	15
6	Schematic of the experimental setup	18
7	Snapshot of the experimental setup.	18
8	Comparison of the amplitude spectra of the fixed LDV and the CSLDV	22
9	Comparison of the waveforms obtained using the CSLVD	23
10	Amplitude spectra of the three DOF	23
11	Effect of scanning frequency on the speckle noise.	24
12	Evolution of the mean noise amplitude vs scan length	24
13	Evolution of the root-mean-square error	26
14	Effect of increasing the scan radius on the modulation signal energy	27
15	Effect of shaker amplitude on error	27
16	Top view of hand tremor experimental setup	28
17	Comparison of time domain waveforms in hand tremor sensing	29
18	Comparison of amplitude spectra in hand tremor sensing	30
19	Schematic of the proposed CSLDV methodology using a linear scan	34
20	Schematic of the experimental setup	36
21	Comparison of the amplitude spectra of the velocity signal	38
22	Variation of the average noise level	38
23	Comparison of the waveforms of fixed LDVs vs virtual sensors	40
24	Comparison of the amplitude spectra of fixed LDVs vs virtual sensors	40
25	Stacked demultiplexed CSLDV waveforms	42
26	Virtual sensors starting from origin	44
27	3D CAD model for the biceps' fixture	48
28	Experimental schematic with complete layout	49
29	Direct wave arrivals at virtual sensors	52

30	Extraction of array of virtual sensors	54
31	Arm length and marking of three fixed LDVs, A, B and C.	54
32	Phase velocity in biceps brachii	55
33	Four different wrist positions and elbow joint angles	56
34	Evolution of elastic wave velocities for four positions	57
A.1	Doppler effect	68
A.2	Michelson interferometry principle	69
A.3	Demodulating the LDV signal	72
B.4	National Instruments data acquisition board	73
B.5	Comparison of baselines for the CSLDV and the fixed LDV	74

CHAPTER I

INTRODUCTION

1.1 Introduction to laser Doppler vibrometer

A laser Doppler vibrometer (LDV) is a non-contact velocity transducer. The use of a laser beam alleviates three main limitations of vibration sensors that must be physically mounted on the test surface, such as accelerometers or strain gauges. First, contact sensors may cause mass loading artifacts that affect the frequency response of the structure, especially when structures are light weight or highly damped non-linear materials such as rubber [9]. Second is the tethering problem, which arises especially when one attempts to mount vibration sensors on rugged or hot surface textures and even rotating objects [6]. Third, electro-magnetic interferences can occur if the vibrations sensors are mounted near electronic devices [30]. A fixed LDV can only measure a single degree of freedom (DOF) of the test surface velocity vibration along the line-of-sight of the laser beam. More sophisticated LDV systems have been developed using multiple laser beams to measure additional DOF. For instance the full three-dimensional surface velocity vector can be measured using three fixed LDV beams [9]. Similarly two fixed LDV beams are typically used to measure angular velocity of rotating surfaces [24, 25, 37].

A complete introduction of LDV principle, Doppler shift frequency, ω_D , interferometry and the demodulation of the Doppler shifted LDV signal is given in appendix A.

1.1.1 Different methods of LDV sensing and their applications

LDV was first used by Yeh and Cummins [75] four decades ago to find velocities of fluid flow as low as 0.007 cm/sec using He-Ne laser 632.8 [nm] wavelength. Durst in 1971 [17] coined the term Laser Doppler Anemometer (LDA) and recognized the difference between Doppler shift and fringe anemometers. A wide range of LDV application covers areas such as structural dynamic testing, biological and clinical diagnostics, fluid-structure interaction, on-line monitoring of industrial plants, acoustics, fault detection and mine detection [9]. Castellini

et al. [10] compared the *in vivo* and *in vitro* results for tooth mobility, (tooth displacement to input force), by using the non-contact LDV method. Goode [22, 21] evaluated the displacement of ear tympanic membrane (0.045 micron at 80 dB of 1 kHz tone) at different sound pressure levels by using fixed LDV sensing method.

A single LDV can be used to perform a discrete scan approach using a series of velocity measurements (time averaging) on a grid of points over the structure under test. Ruzzene [47] obtained the full wavefield measurement using the discrete scan LDV technique (on user-defined grid) for fault detection in an Aluminum structure as an application to Structure Health Monitoring (SHM). Tomasini [45] analyzed the human hand-arm vibration response using discrete scan LDV (on grid points) with sinusoidal excitation of 250 Hz (human-machine interface). But this discrete (or sequential) scanning LDV approach is slow, does not permit synchronized (i.e., simultaneous) vibrations measurements over an extended area and requires the use of a repeatable surface excitation from one measurement to the next.

1.1.2 Continuous Scanning LDV (CSLDV)

A straightforward approach for synchronized vibration measurements is to jointly use multiple laser beams. But current multi-beam LDV systems are expensive and the projected pattern formed by the laser beams onto the surface is pre-determined using a fixed mask and thus can not be easily re-configured in near real time [3].

An alternative approach to complex LDV systems with multiple laser beams, is the use of a continuous scanning LDV (CSLDV) relying on a *single* laser beam moving along a periodic pattern over the test surface. The mirror is computer controlled and can generate different types of waveforms depending upon the vibration measurement requirements. This technique is known as a continuous scanning laser Doppler vibrometry (CSLDV). It has some potential advantages over a fixed point LDV. For instance, multiple DOF of vibration can be analyzed using CSLDV technique. The measurement of number of DOF depends upon the type of scanning waveforms which is further explained in Section 1.1.3. Another benefit of using CSLDV method is that the laser scan can act as an array of transducers (LDVs) measuring velocity vibrations of surfaces. Sriram et al. [61, 63, 64, 62] worked on

the CSLDV to determine the mode shapes and the Frequency Response Functions (FRF) of a structure. Further research was conducted at the Imperial College in London by Stanbridge [65], who worked on finding the mode shapes and the FRF of a steel plate using the CSLDV. Ewins and Martarelli published results about the CSLDV and speckle noise [34] which explained how a slow moving mirror (0.2 Hz to 20 Hz) can find the surface vibration of a structure, vibrating sinusoidally at a higher frequency (> 300 Hz). Stanbridge and Ewins [65] found mode shapes of a harmonically exciting surface using line, area and circular scan patterns with low scanning frequency (\approx a few Hz) compared to the excitation frequency (≈ 1 kHz). Allen proposed a methodology improvements (“lifting method”) to estimate the mode shapes by impact excitation using this non-contact CSLDV technique [1].



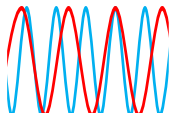

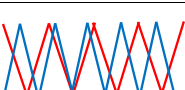
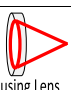
Scan patterns	Mirror driver signal	Schematic of scan types	DOF measurement
Line Scan	Sine or triangular Wave		One translational, one rotational
Circular Scan	Sine and cosine waves at same frequency		One translational, two rotational
Lissajous trajectory (Area Scan)	Two Sine waves at different frequencies		One translational two rotational with more control over rotational measurement
Circular Area Scan	A sine wave and a triangular wave at different frequencies		One translational two rotational with more control over rotational measurement, round structure application
Area Scan	2 triangular waves at different frequencies		One translational two rotational with more control over rotational measurement
Conical Scan	By focusing a circular scan	 Focusing Lens	Three translational in x-y-z directions

Figure 1: Major types of scans, their driver signals and advantages, adapted from Martarelli [34].

1.1.3 Types of CSLDV used in this research

CSLDV techniques can be divided in two main categories which are referred hereafter as “short-scan” (i.e., local) or “long-scan” (i.e., global) techniques- depending on whether the laser scan’s dimensions are smaller or larger than the characteristic wavelength of the measured surface vibrations [65, 35]. Short-scan CSLDV techniques allow measuring translational and angular vibrations -for up to five-DOF-at a single point on a structure using a variety of scan patterns (e.g., linear, circular, conical ...) [66, 65, 35]. On the other hand “long-scan” CSLDV technique are used to simultaneously measure single-DOF vibrations (e.g., normal translation velocity) at multiple locations over the test surface [65, 1, 62]. These distributed velocity measurements can be further processed using various approaches to extract mode shapes, natural frequencies and damping ratios of the test structure for modal analysis purposes [61, 63, 64, 65, 71, 67, 1, 2, 74]. This research work focuses both the short scan (rigid body models) as shown in Figure 2a,b and the long scan Figure 2c for bio-mechanical application which describes how forces produced by human skeletal muscles affect the elastic stiffness of muscles. Figure 2 shows points A,B,C and D which are used for fixed lasers in order to validate the measurements obtained from the CSLDV.

Each scan type has the ability to measure more than one DOF of vibration unlike LDV with a fixed laser beam. For instance, a line scan can measure one translational and one rotational DOF of velocity vibration (see Figure 2a). A circular scan has the ability to measure one translational and two rotational degrees of velocity vibration (see Figure 2b). Additionally, the line and circular scans will be presented in detail hereafter, as they will be the main scan types, used in this research. A conical scan can measure three translational DOF of velocity vibration i.e., along x-y-z-axes. Lissajous scan is a scan in which one mirror axis has a certain frequency and the other one has a different frequency which is related as a harmonic of each other. This scan can potentially measure up to three-DOF, one translational and two rotational as in the case of the circular scan pattern, but allows more control on each rotational DOF by controlling the frequency of each mirror axis individually.

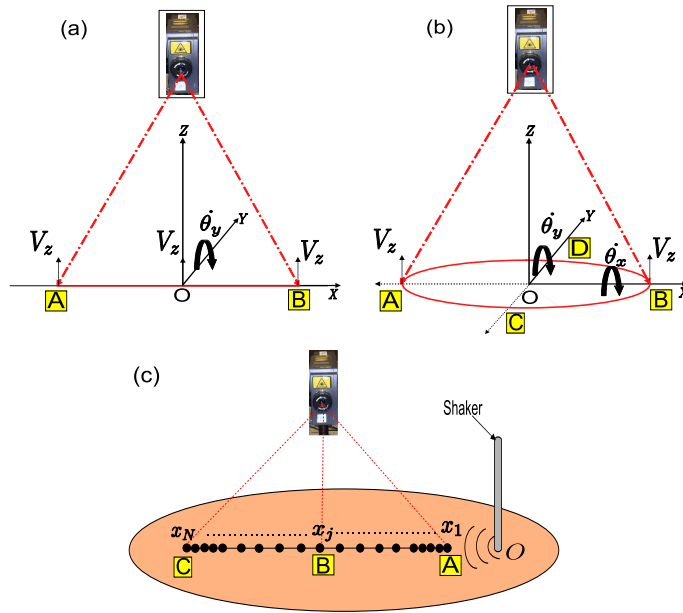


Figure 2: (a) Short line scan schematic describing two types of DOF velocity measurement, one linear (V_z , normal velocity) and one angular ($\dot{\theta}_y$, angular velocity about y-axis). (b) Short circular scan schematic demonstrating three types of DOF velocity measurement, one linear (V_z , normal velocity) and two angular ($\dot{\theta}_x$, angular velocity about x-axis and $\dot{\theta}_y$, angular velocity about y-axis). (c) Long line scan schematic showing an array of virtual sensors (x_1 to x_N) inside the long line CSLDV for normal velocity measurements.

Reflected laser beam wavelets
 $= f(\text{space, time, spot size, wavelength, phase})$

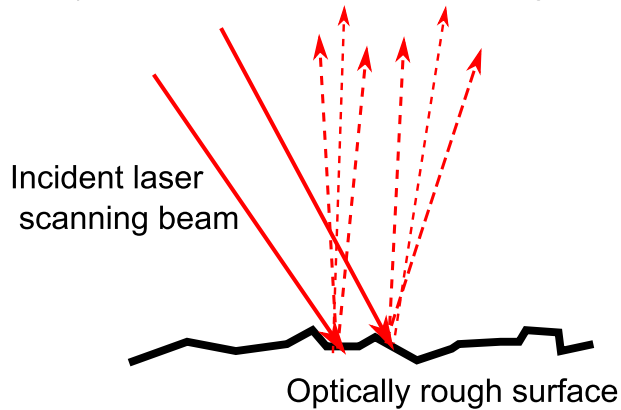


Figure 3: Incoming light rays reflecting back in different directions from an optically rough surface, carrying different phase information, interfere constructively and destructively, forming speckles on the laser photo-detector, (adapted from Sracic [59]).

1.2 Speckle noise

The main practical limitation of CSLDV over conventional fixed LDVs is the greater influence of speckle noise. Speckle noise is generated when a coherent light source, such as a

laser, is reflected back from rough surfaces, i.e., surfaces with significant topographic variations compared to the optical source's wavelength [68]. Speckles are not produced when laser strikes a specular (mirror-like) surface. However, usually surfaces are diffusive and rough on the scale of the optical wavelength i.e., the imperfections in the surface are significant as compared to the wavelength of light. This diffusive surface causes constructive and destructive interference of the component wavelets of the back scattered laser light. Figure 3 shows that the back scattered light is primarily a function of space, time, the wavelength of light and the phase it carries. The spatial and temporal characteristics of the speckle noise depend, among others, on the diameter (spot size) of the laser beam, the reflectivity and the physical properties of the test surface, the amplitude of the measured vibrations, the sampling frequency and the detector sensitivity [36, 59]. The back scattered wavelets interfere at the detector surface and produce a varying intensity image, bright (high intensity) and dark (low intensity) regions known as "speckle pattern". A dark speckle reduces the signal to noise ratio (SNR) while a bright speckle is good for better SNR.

The variations of the speckle amplitude appear as random parts of the test surface, but they occur at the same positions during a periodic scan of the CSLDV beam with good repeatability [35]. These periodic components of the speckle noise can become significant, especially at frequencies close to the main scanning frequency of the laser beam and its related harmonics [42]. Speckles are generally periodic if the scanning frequency is periodic and these periodic noise peaks are not due to the structural resonances but due to periodic speckles and therefore these are known as "pseudo vibrations" [46]. If the surface is moving and a fixed LDV is shining at a fixed point then speckles will also move and this phenomena is known as "boiling" [68]. When a laser is scanning on a vibrating surface, it will change its phase which causes noise spikes in the velocity signal other than the periodic speckle peaks which are known as non-periodic speckle noise. Minimizing or mitigating the effects of speckle noise is thus the key to ensure accurate vibration measurements from the CSLDV systems.

1.3 Benefits of CSLDV for bio-mechanical application

Figure 4 shows a comparison of using accelerometers with a non-contact method of vibration measurements using a CSLDV technique to measure vibrations of the biceps brachii muscle. As mentioned earlier in Section 1.1, accelerometers or other contact sensors have problems such as mass loading effect, tethering problems, cable dynamics involved and the long setup time requirement. These limitations are overcome using the non-contact way of CSLDV. It is very easy to use CSLDV which gives multiple locations measurements by a single LDV sensor steered by a mirror. The idea is to implement this technique for getting the dynamic elastography Imaging (Section 1.5) of human skeletal muscles using external vibrating source. The oscillations of skeletal muscle fibers are below 100 Hz [41, 4, 14] at different levels of muscle maximum voluntary contraction (MVC) which put a limitation on the scan rate of the CSLDV to be at least 200 Hz (Nyquist criteria).

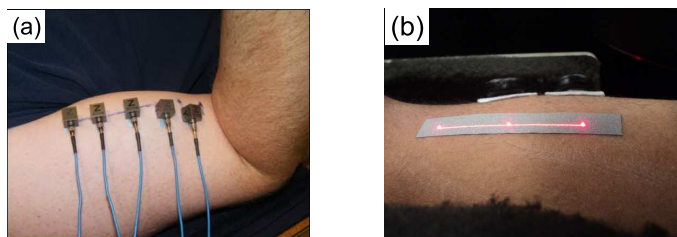


Figure 4: (a) Existing technique [4, 14] of skin-mounted accelerometers used for finding surface mechanomyograms. (b) Proposed technique for finding surface forced vibrations by using a long line CSLDV. The technique usually requires an adhesive reflective tape.

1.4 Elastic properties of skeletal muscles

Skeletal muscles are made up of striated fibers that attach to the skeleton via tendons and are responsible for voluntary body movements [73]. Measuring the in vivo elastic properties of muscles (e.g., stiffness) can provide a means for diagnosing and monitoring muscular activity and force generation: muscles typically become harder during contraction due to physiological changes. Indeed, muscle stiffness is expected [19, 56, 8] to change during contraction. Thus, mechanical properties of skeletal muscles have been used as essential parameters to predict muscle functional properties and to assess the therapeutic progress and recovery from musculoskeletal and neuromuscular disorders [18]. For instance, those

patients with musculoskeletal and neuromuscular disorders (e.g., stroke, spinal cord injury, and multiple sclerosis) frequently have heightened “muscle tone” that limits their movement capability [51]. Currently, muscle tone is most commonly sensed qualitatively with manual palpation at the muscle surface and thus can only be judged subjectively by clinicians. Additionally laboratory measurements of the viscoelasticity of isolated (skinned) muscle fibers or sarcomeres, are invasive and cannot describe the in vivo mechanical behavior of whole muscles due to the influence of connective tissues [76].

Indeed, little is known about how muscle mechanical properties vary quantitatively during contraction (even for healthy individuals) or during physical rehabilitation treatments for patients with musculoskeletal and neuromuscular disorders, mainly because noninvasive and quantifiable techniques for measuring muscle mechanical properties are not readily available in clinical practice [23]. Furthermore, due to muscle redundancy, several muscles typically contribute to force generation (or torque output) even for simple task. Thus developing a methodology to estimate the actual force produced by individual muscle (or muscle groups) remains an open research question in biomechanics [8].

1.5 Dynamic elastography

Dynamic elastography is a technique by which an external source of vibration is coupled with the skeletal muscle and the analysis of wave pattern describes the wave propagation velocity of mechanical vibrations (e.g., shear waves) to estimate the local stiffness of soft tissues (e.g., faster velocity indicates stiffer material) [12, 23]. Dynamic elastography imaging techniques use an active vibration source of some type (e.g., vibrating probe at muscle extremity or ultrasonic radiation force) to generate propagating low-frequency vibrations (typically shear waves) along the tested muscle [23, 27] and most commonly either ultrafast ultrasound recordings [32, 15] or magnetic resonance images [39, 16] track these propagating shear vibrations and measure their velocity. Ongoing studies have started to demonstrate the clinical applicability of dynamic elastography-such as magnetic resonance elastography or ultrafast ultrasound elastography [23]- for quantitative diagnosis of skeletal muscle mechanical properties and to develop databases of their viscoelastic parameters [5, 43, 19, 56].

Based on these recent technological breakthroughs, sophisticated active elastography imaging systems are now being commercialized. However, these commercial systems have inherent limitations since they require, 1) sophisticated and expensive imaging equipments ($> \$1,000,000$ for MRI system and $\approx \$ 200,000$ for ultrasound elastography system), and potentially 2) complex signal processing, to record and analyze muscle vibrations. Thus, these requirements may increase the complexity and costs of elastography imaging thus potentially limiting its clinical use. Furthermore, these commercial systems offer a good spatial resolution of the stiffness measurements over the measurement area. However, clinicians may only need to measure a global value of the stiffness of the tested skeletal muscles to assess its net force output or its overall muscle tone, and thus clinicians may not need in practice the full spatial resolution of the local stiffness fluctuations offered by these sophisticated commercial systems.

1.6 Motivation and objectives

The main objective of this thesis is to develop a Continuous Scanning Laser Doppler Vibrometry (CSLDV) technique to measure multiple DOF of vibration of the surface of interest. The proposed methodology is cost effective since for the measurement of multiple DOF of vibration, multiple LDVs are required. For instance, at least two fixed point LDVs are required to find one translational and one angular DOF of vibration which increases the system cost.

One of the motivations of this research is to use a “short-scan” CSLDV technique for measuring multiple DOF of natural human body vibrations on specific joints or limbs. This laser-based technique offers a simple, easy to set-up and non-contact alternative for sensing small human body parts (e.g., fingers, tendons, small muscles) onto which vibration sensors can not be skin-mounted easily or at all. This CSLDV technique could potentially enhance the applicability and performance of various applications relying on forced feedback control systems and sensing of fine motor tasks such as remote surgery, haptic technology and prosthetic control. In particular, natural vibrations of skeletal muscles during voluntary contractions are typically characterized as random and broadband vibration with a main

frequency content below 100 Hz, this upper frequency being primarily limited by the firing rate of muscle fibers [41, 4, 14, 40, 48, 50]. However previous “short-scan” CSLDV studies mainly reported on multiple DOF measurements for modal testing applications and thus focused on measuring harmonic translational and angular vibrations at frequency significantly higher (e.g., $f > 100$ Hz) than the scanning frequency of the laser beam (e.g., 0.2 to 20 Hz) using a demodulation algorithm for specific Fourier components [66, 65, 67]. Consequently, in order to use the short-scan CSLDV technique for measuring multiple DOF of natural skeletal muscle vibrations, this research presents instead a variant of the CSLDV demodulation algorithm used in these previous studies, to directly extract random and broadband translational and angular vibrations with low frequency content (i.e., < 100 Hz from human body tremors during fatiguing tasks) from the CSLDV signal using a high scanning frequency (i.e., 200 Hz here) of the laser beam over the test surface.

Another objective of this work is the development of simple, affordable, noninvasive and in vivo elastography for assessing the average stiffness value of skeletal muscles. This “laser elastography” technique could accelerate the transition to clinical practice and thus ultimately improve and simplify the objective clinical diagnosis of musculoskeletal and neuromuscular disorders. In order to achieve the non-invasive and in vivo elastic properties of human skeletal muscles, a long line CSLDV technique will be implemented. The idea is to obtain synchronized measurements of broadband surface vibrations by continuously scanning a *single* laser beam at high speed along an arbitrary periodic pattern over the test surface [60, 1, 11]. This CSLDV technique will rely on demultiplexing the CSLDV signal to extract surface vibration measurements along the periodic scan pattern traced by the optical beam, thus creating in effect an array of virtual velocity sensors over the scanned surface. This CSLDV technique requires that the scan frequency be at least twice higher than the highest vibration frequency of the test surface in order to avoid any aliasing issues as stated by the Nyquist sampling theorem [1, 11, 55]. Furthermore this CSLDV methodology is applicable even if the source signal occurs once and is not repeatable (e.g., bandlimited random excitations [74]). Thus, this technique is especially advantageous for sensing natural vibrations of the human body at multiple locations (e.g., along small muscles) as it does not

require traditional skin-mounted sensors (e.g., accelerometers array), which eliminates mass artifacts and the setup time to attach those sensors as discussed in Section 1.3. Ultimately, this CSLDV technique could then be used to provide a simple, affordable, noninvasive and in vivo elastography modality for quantitative measurements of muscles' tone (or stiffness) and thus potentially improve the objective diagnosis of musculoskeletal and neuromuscular disorders in the clinical practice.

Finally, it should be noted that previous studies have primarily focused on using this CSLDV technique for modal analysis purposes by identifying the mode shapes, natural frequencies and damping ratios of relatively large structures such as metal beams[60, 1, 11] or wind turbine's blade [74]. Furthermore, the experimental method used in previous research for generating a long line CSLDV [1, 74, 59] was different with respect to the laser vibrometer and type of excitation (impact in their case). These studies used a Polytec TM PSV 400 which has a built in mirror and more expensive than our system which is a combination of a simple Polytec TM PDV 100 and a piezoelectric two-axes fast scanning mirror (PhysikTM InstrumenteTM, Model S-334).

1.7 Structure of thesis

Chapter II introduces and implements the short scan CSLDV technique for measuring the multiple DOF of velocity vibrations. The rigid body models for both short line and circular scans are presented here. First part of this chapter describes the analytical formulae for extracting the translational and angular broadband vibrations of the test surface from the velocity output of a single CSLDV performing either line or circular scans. It explains the complete experimental setup required for the development of this CSLDV technique. It validates the proposed CSLDV technique on soft gel samples (mimicking human body soft tissues) excited by broadband vibrations ($10 \text{ Hz} \leq f \leq 50 \text{ Hz}$) using pairs of fixed LDVs. The effect of speckle noise on the measurement error is also quantified. Next, this CSLDV technique is applied on a human subject to measure the translational and angular velocities resulting from a hand tremor during a fatiguing task against the gravity. Finally, it summarizes the findings and conclusions drawn from this study.

Chapter III demonstrates the applicability of long line CSLDV technique for measuring low-frequency ($f < 100$ Hz) flexural waves propagating over gelatin samples (mimicking human body soft tissues) with high spatial resolution (\approx mm) over a 5 cm scan length. The first part of the chapter presents the experimental setup for this CSLDV technique. It explains the demultiplexing methodology for extracting the synchronized surface vibrations from the CSLDV signals. It presents the validation of the proposed CSLDV technique using the conventional method of the fixed LDVs. Sources of error and the limitations are explained in detail. Finally, the stiffness of gel is found using this long line CSLDV technique.

Chapter IV validates and implements this long line CSLDV methodology to perform elastography measurements [12, 23], based on the apparent velocity of low-frequency flexural waves, propagating along the biceps brachii axis during isometric voluntary contractions at various MVC levels. The first part of the chapter explores the design of the fixture for biceps contraction force and effect of biceps isometric contraction on the stiffness level for ten healthy male subjects. Second part describes the effect of four different wrist positions and elbow joint angles for the bicep isometric contraction on the measured velocities for 14 male subjects. Finally, there is discussion about the conclusion and the summary for this chapter.

CHAPTER II

SHORT SCAN

Short scan CSLDV is a technique which has its ability to measure multiple DOF of velocity vibration. During a short scan the test surface is assumed to act as a rigid body. As described in Chapter 1, the name short in the short scan is a relative term with respect to the spatial wavelength of the flexural wave over a surface of interest. If the scan length is smaller than the spatial wavelength of the surface wave then the scan is known as “short scan”. This is a non-contact way of vibration measurement using a single LDV, which has its advantage over other skin-mounted sensors. The rigid body models for both short line and circular CSLDV methodology will be presented in this chapter. These models provide the measurements of multiple DOF of natural human body vibrations on specific joints, skeletal muscles or on limbs. The goal of this chapter is to validate this short scan CSLDV rigid body models on a gel (mimicking human body soft tissues) surface and then implement it on human body joints to measure multiple DOF of vibration. This chapter will present analytical formulae for extracting translational and angular broadband vibrations of the test surface from short scan (line or circular). These measurements from the CSLDV will be validated against the measurements obtained by the conventional method of fixed LDVs. A custom made soft gel will be used as a test surface excited by broadband vibrations ($10 \text{ Hz} \leq f \leq 50 \text{ Hz}$). The reason for the selection of low frequency broadband excitation on the gel surface is because of its implementation on human skeletal muscles, which have the firing rate below 100 Hz [41, 4, 14, 40, 48, 50]. Finally, this technique will be applied on human subject to measure the translational and angular velocities resulting from the hand tremor during a fatiguing task.

2.1 Theory

2.1.1 Geometry for line and circular short scans

As mentioned in the introductory section, an LDV allows for non-contact measurement of the velocity vibration of a given reflective surface. More specifically, a single LDV only measures the projection of the surface velocity vector onto the laser beam direction. For short-scan CSLDV techniques, the orientation of the laser beam is continuously varied to effectively measure multiple DOF of the surface vibrations at a single point, typically corresponding to the center of the laser scan [66, 65, 35]. This research study uses two short-scan patterns—the line scan and the circular scan (see Figure 5)—to measure both translation and angular surface velocities. For the circular scan, the instantaneous positions $x(t)$ and $y(t)$ of the laser beam are assumed to follow a sinusoidal pattern at the same scanning frequency Ω .

$$x(t) = R \cos(\Omega t) \quad (1)$$

$$y(t) = R \sin(\Omega t) \quad (2)$$

where R represents the radius of the circular scan [66, 65, 35]. The short line scan (of extent $2R$) is obtained by setting $y(t) = 0$ and keeping $x(t)$ the same. It can be noted that the geometry of the scan pattern of the CSLDV can be readily modified by changing the amplitude and time-dependence of the instantaneous positions $x(t)$ and $y(t)$ of the laser beam. For instance, elliptical Lissajous patterns can be obtained by selecting harmonic displacements $x(t)$ and $y(t)$ with different amplitude and frequencies [65, 35].

Assuming that the small scan area behaves as a rigid body (i.e., as a non-deforming planar surface), the velocity signal $V(t)$ of the CSLDV performing a short line scan (Figure 5a) is given by [66, 65, 35]:

$$V(t) = V_z(t) + x(t)\dot{\theta}_y(t) \quad (3)$$

where $V_z(t)$ is the normal velocity of the surface (along the vertical z -axis) at the middle point O of the scan, $x(t)$ is the instantaneous position of the laser beam along the x -axis and $\dot{\theta}_y(t)$ is the angular velocity of the surface about the y -axis at the same point O . Similarly, the velocity signal $V(t)$ of the CSLDV performing a short circular scan (Figure 5b) can be

expressed as [66, 65, 35]:

$$V(t) = V_z(t) + x(t)\dot{\theta}_y(t) + y(t)\dot{\theta}_x(t) \quad (4)$$

where $y(t)$ is the instantaneous position of the laser beam along the y-axis and $\dot{\theta}_x(t)$ is the angular velocity of the surface about the x-axis at the center point O of the circular scan. Thus in practice, line scans allow measurement of two DOF (one translation velocity and one angular velocity) using a one-dimensional scanning mirror to deflect the laser beam. On the other hand, circular scans allow measuring three DOF (one translation velocity and two angular velocities) but require the use of a two-dimensional scanning mirror.

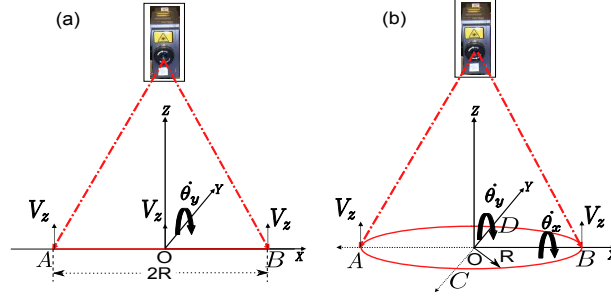


Figure 5: Rigid body models used in CSLDV. (a) A line scan of length $2R$ along the x-axis allows measurement of the normal velocity $V_z(t)$ and the angular velocity $\dot{\theta}_y(t)$ about the y-axis. (b) A circular scan of radius R in the x-y plane allows measurement of the normal velocity $V_z(t)$ and two angular velocities $\dot{\theta}_y(t)$ about the y-axis and $\dot{\theta}_x(t)$ about the x-axis.

2.1.2 Data processing for extracting the translational and angular broadband vibrations from the CSLDV signal

Using a radio telecommunication analogy, the angular vibrations $\dot{\theta}_y(t)$ and $\dot{\theta}_x(t)$ in Eqs. (3) and (4) act as an amplitude modulation factors of the sinusoidal carrier signals $x(t)$ or $y(t)$ oscillating at the scanning frequency Ω of the laser beam. Note also that the signals $x(t)$ and $y(t)$ have a quadrature phase relationship. Based on these considerations, previous studies [66, 65, 35] have proposed to use a demodulation algorithm of the CSLDV signal given by Eqs. (3) and (4) to extract both normal and angular velocities $V_z(t)$, $\dot{\theta}_y(t)$, and $\dot{\theta}_x(t)$. Their proposed demodulation algorithm supposes that the tested structure undergoes a sinusoidal vibration, say at frequency ω , such that it can be assumed that all DOF are sinusoidal at the same frequency (though not necessarily in phase). In this case, if Ω denotes the laser

beam scan frequency and if $\Omega \ll \omega$, the resulting CSLDV signal given in Eqs. (3) and (4) comprises three distinct harmonic components: at frequencies ω , $(\omega + \Omega)$ and $(\omega - \Omega)$. The complex amplitudes of the angular and translation velocities at the frequency ω can then be individually retrieved by solving the system of equations derived from Eqs. (3) and (4) which links the three measured harmonic components. It should be noted that because the harmonic component at $(\omega - \Omega)$ needs to be isolated for this demodulation algorithm to work, the scanning frequency Ω must then be significantly lower than the vibration frequency ω as pointed out by the previous studies [66, 65, 35]. This demodulation algorithm can be readily extended to measured vibrations composed of multiple spectral components as long as these components are clearly separated in the Fourier domain such that the modulated sidebands at $\omega_i \pm \Omega$ don't overlap for different center frequencies ω_i . However, this harmonic-based demodulation algorithm is not readily suitable for broadband vibrations with a continuous spectrum, such as random continuous vibrations as mentioned in the introductory section.

Consequently, this study presents an alternative formulation of the aforementioned demodulation algorithm to extract instead both translational and angular broadband vibrations of the test surface using a single CSLDV performing a circular scan [see Eq. (4)]. First, the normal vibration $V_z(t)$ and angular vibrations $\dot{\theta}_y(t)$ and $\dot{\theta}_x(t)$ are assumed to be continuous waveforms within a limited frequency bandwidth $[f_1, f_2]$. Second, the scanning frequency Ω of the laser beam is assumed to be at least twice the upper frequency f_2 (i.e., $\Omega > 2f_2$) to avoid any overlap in the modulated side-bands in the CSLDV signal. Under these assumptions, the final expression of the broadband velocity signal $V(t)$ of the circular scan CSLDV obtained by combining Eqs. (1) to (3) contains three main components in the frequency domain (e.g., as shown in the amplitude spectrum displayed on Figure 8).

- A narrow-band spectral line at the frequency $f = \Omega$
- A broadband component for frequencies $f_1 \leq f \leq f_2$ associated with the the normal vibration $V_z(t)$
- A broadband component for frequencies $\Omega - f_2 \leq f \leq \Omega - f_1$ associated with the angular vibrations $\dot{\theta}_y(t)$ and $\dot{\theta}_x(t)$

The frequency content of the third component can be determined mathematically based on the convolution theorem for the Fourier transform, which relates here the product of a broadband function and harmonic function in the time domain [e.g., the term $\dot{\theta}_y(t)x(t)$ in Eq. (3)] to the convolution of their Fourier transform. Consequently, the normal velocity and two angular vibrations of the test surface can be extracted from the velocity signal $V(t)$ of the CSLDV using the following three relationships

$$V_z^{scan}(t) = filter [V(t)], \quad (5)$$

$$\dot{\theta}_y^{scan}(t) = 2/R \times filter [V(t) \cos(\Omega t)], \quad (6)$$

and

$$\dot{\theta}_x^{scan}(t) = 2/R \times filter [V(t) \sin(\Omega t)], \quad (7)$$

where the operator, *filter* refers to a band pass filter operation in the frequency band $[f_1, f_2]$. Equations (6) and (7) are obtained using the orthogonality property of the harmonic “carrier signals”, while $x(t)$ and $y(t)$ which are in phase quadrature. Another practical benefit for using the bandpass filter is to eliminate the speckle noise at frequencies above the main frequency band of the surface vibrations, and especially the high amplitude spectral line centered around the scanning frequency $f = \Omega$.

2.2 *Experimental validation*

The proposed methodology in Section 2.1 for measuring both translation and angular velocities using a single CSLDV is tested here on a gel sample undergoing low-frequency broadband vibration.

2.2.1 **Experimental setup**

A description of the experimental setup shown on Figure 6a and Figure 7 is given hereafter. A gel sample, made from commercially available gelatin with a stiffness (Young’s modulus) of approximately 4.5 kPa, (mimicking human body soft tissues), is excited by an electrodynamic mini-shaker (B & KTM Model 4810) in the frequency band [10 Hz to 50 Hz]. However, this gel medium is very transparent and diffusive; this makes it a poor reflector of the laser

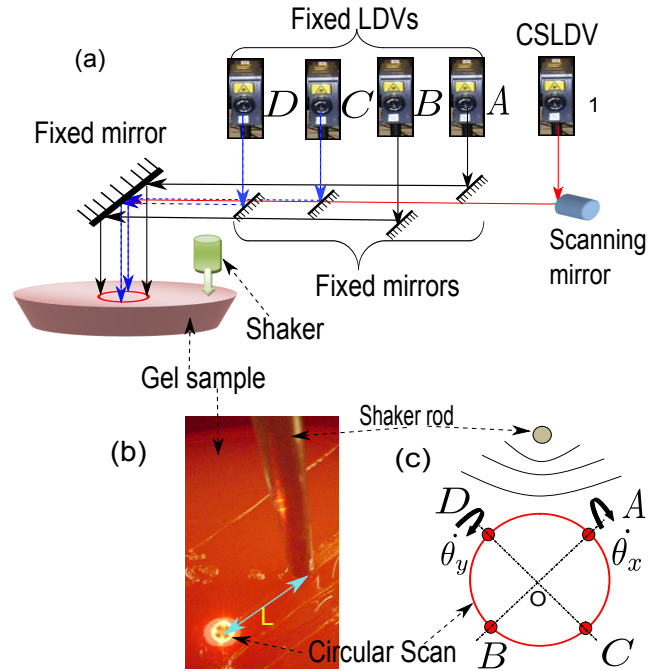


Figure 6: (a) Side view schematic of the experimental setup. Arrows indicate the optical paths of the 5 laser beams used in this study. (b) Snapshot of the actual experiment for a circular scan pattern on the gel surface. (c) Top view schematic of the circular scan showing the orientation of the measurements points A-D of the four fixed LDVs with respect to the shaker rod. The circular scan pattern of the CSLDV is also indicated (same geometry as in Figure 5).

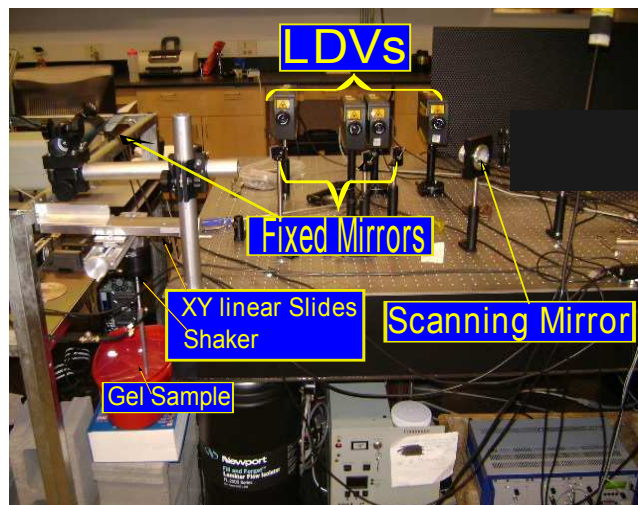


Figure 7: Snapshot of the experimental setup.

beam, therefore a piece of retro-reflective tape is used to enhance its reflectivity. Hence for circular scans, a thin ring-shaped piece of retro-reflective tape (3MTM ScotchliteTM - 9810 multipurpose tape) is fixed onto the gel. The ring thickness is 3 mm (see Figure 6b). For line scans, a 3 mm thin rectangular-shape is used instead. The LDV (PolytecTM Model PDV 100) labeled as 1 on Figure 6a is used to continuously scan the gel surface along the retro-reflective tape. In order to satisfy the rigid body model used in Eqs. (3) and (4), the maximum scan length $2R$ used in this study was less than 20 mm which approximately corresponds to a half-wavelength of the low-frequency flexural waves excited by the shaker over the gel's surface (this wavelength was estimated as the ratio of the propagation velocity of the flexural wave over the gel surface-measured as 1 m/s here- to the shaker excitation's center frequency of 30 Hz). A description of the experimental setup shown on Figure 6a and Figure 7 is given hereafter. A gel sample, made from commercially available gelatin with a stiffness (Young's modulus) of approximately 4.5 kPa, (mimicking human body soft tissues), is excited by an electrodynamic mini-shaker (B & KTM Model 4810) in the frequency band [10 Hz to 50 Hz]. However, this gel medium is very transparent and diffusive; this makes it a poor reflector of the laser beam, therefore a piece of retro-reflective tape is used to enhance its reflectivity. Hence for circular scans, a thin ring-shaped piece of retro-reflective tape (3MTM ScotchliteTM - 9810 multipurpose tape) is fixed onto the gel. The ring thickness is 3 mm (see Figure 6b). For line scans, a 3 mm thin rectangular-shape is used instead. The LDV (PolytecTM Model PDV 100) labeled as 1 on Figure 6a is used to continuously scan the gel surface along the retro-reflective tape. In order to satisfy the rigid body model used in Eqs. (3) and (4), the maximum scan length $2R$ used in this study was less than 20 mm which approximately corresponds to a half-wavelength of the low-frequency flexural waves excited by the shaker over the gel's surface (this wavelength was estimated as the ratio of the propagation velocity of the flexural wave over the gel surface-measured as 1 m/s here- to the shaker excitation's center frequency of 30 Hz).

The LDV beam is deflected using a two-axes fast steering mirror (1/2 inch diameter, maximum angular deflection of 2.86° or 50 mrad in closed feedback control loop), mounted on piezoelectric actuators (PhysikTM InstrumenteTM Model S-334). Furthermore, the short

scan length used in this study ($R < 10$ mm here) ensured that the laser beam remains nearly perpendicular to the gel's surface at all times, as assumed when deriving Eq. (3). For all experiments, the fast scanning frequency of this mirror is set to $\Omega = 200$ Hz, which is well below the first resonance frequency of the oscillating mirror (1000 Hz). The effective scanning velocity for a 5 mm short line and circular scan is 180 cm/s. The circular or line scan pattern of this CSLDV is reflected using a fixed mirror-mounted at a 45° angle to achieve normal incidence onto the horizontal gel surface. The four other LDVs-labeled as A–D on Figure 6a - are used to validate the three-DOF (i.e., one translational velocity and two angular velocities-see Figure 5b), measured by the circularly scanning LDV. As depicted on Figure 6c, the four fixed laser beams (A–D) are projected along a normal incidence and 90° apart on each quadrant of the ring-shaped retro-reflective tape using two successive reflections on fixed mirrors oriented at 45° . Consequently, the estimated normal velocity, $V_z^{fix}(t)$ and angular velocities $\dot{\theta}_y^{fix}(t)$ and $\dot{\theta}_x^{fix}(t)$ of the gel surface can be obtained from the measured velocities $V_A(t), V_B(t), V_C(t), V_D(t)$ of the four fixed LDVs using:

$$V_z^{fix}(t) \approx \frac{V_A(t) + V_B(t) + V_C(t) + V_D(t)}{4}, \quad (8)$$

$$\dot{\theta}_y^{fix}(t) = \frac{\partial V_z(t)}{\partial x} \approx \frac{V_A(t) - V_B(t)}{2R}, \quad (9)$$

and

$$\dot{\theta}_x^{fix}(t) = \frac{\partial V_z(t)}{\partial y} \approx \frac{V_C(t) - V_D(t)}{2R} \quad (10)$$

These formulae for the translation and angular velocities of the gel surface obtained from the fixed LDVs using Eqs. (8) to (10) are used to validate the estimates of the same three velocities derived directly from the CSLDV measurement $V(t)$ using Eqs. (5) to (7). Note that for the case of line scans, only two fixed LDVs are needed for experimental validation (e.g., LDVs A and B to validate the CSLDV measurements obtained for a line scan along the x-axis). All fixed and scanning LDVs as well as reflective mirrors were mounted on an optical table (Newport Model RS2000-46-8) supported by pneumatic Stabilizer Isolators

(Newport Model S-2000 series). Furthermore, the settings of all LDVs were set to the sensitivity scale of maximum velocity (500 mm/s = 4 V), with a low pass filter of 1 kHz. A National Instruments data acquisition board, (cDAQ-9178 with eight input/output module slots) was used to simultaneously sample all LDVs signals with a sampling rate of 10 kHz using the labVIEW software (see appendix B.1).

2.2.2 Experimental comparison between fixed LDV and continuously scanning LDV measurements

The gel surface was excited with a 7 s long linear frequency modulation (LFM)[29] waveform in the frequency band [$f_1=10$ Hz to $f_2=50$ Hz]. The distance, L , between the shaker tip and the center of the circular scan was 10 cm. The recordings of all five LDVs signals (fixed and scanning) were triggered by the onset of the shaker's excitation and lasted for 10 s (i.e., 3 s beyond the end of the shaker's excitation) to fully capture the damped vibration response of the gel. Figure 8 compares the frequency spectra of the velocity signals $V(t)$ of the CSLDV (dashed line) performing a circular scan (radius $R = 5$ mm) to the velocity signal $V_A(t)$ of the fixed LDV (plain line). As discussed in Section 2.1.2, the harmonic peak at the scanning frequency $\Omega = 200$ Hz as well as modulation sidebands between [150 Hz to 190 Hz] and [210 Hz to 250 Hz] corresponding to the angular velocities of the gel surface are clearly visible on the CSLDV spectrum. The amplitude of the harmonic at $\Omega = 200$ Hz (e.g., see Figure 8) gives a measure of the strength of the repeatable component of the speckle noise [58]. Furthermore, the amplitude spectra of the fixed LDV and CSLDV closely overlap in the shaker's main frequency band [10 Hz to 50 Hz]. This portion of their spectra correspond to the normal velocity V_z of the gel surface. Finally, the speckle noise level (as estimated from the amplitude of the signal-free frequency band $B_n=[80$ Hz-120 Hz]) is close to 5×10^{-3} mm/s/Hz for this experimental setup (see Figure 12a). This noise amplitude is less than 1 % of the maximum value of the surface velocity V_z in the frequency band of [10 Hz to 50 Hz].

To validate the CLSDV methodology presented in Section 2.1, Figures 9 and 10 show both the time-domain signals and their corresponding amplitude spectra for all three DOF of interest, i.e., the normal velocity $V_z(t)$ and angular velocities $\dot{\theta}_y(t)$ and $\dot{\theta}_x(t)$, estimated

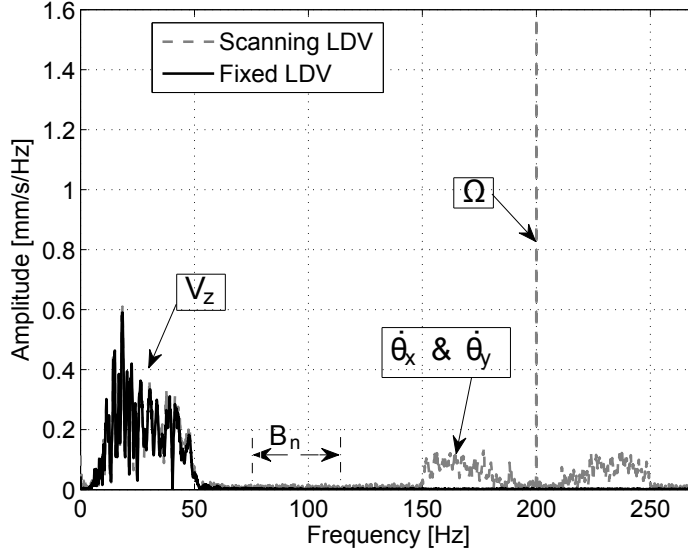


Figure 8: Comparison of the amplitude spectra of the fixed LDV and the CSLDV when the gel surface is excited by an LFM signal (from 10 Hz to 50 Hz) while the CSLDV performs a 5 mm circular scan. The sidebands centered around the scanning frequency $\Omega = 200$ Hz of the laser beam are determined by the amplitude spectra of the angular velocities $\dot{\theta}_x(t)$ and $\dot{\theta}_y(t)$. The signal-free frequency band $B_n = [80 \text{ Hz}-120 \text{ Hz}]$ is used to estimate the mean noise floor level of the measurements.

either from the single CSLDV using Eqs. (5) to (7) or from the four fixed LDVs using Eqs. (8) to (10). Overall, the measurements of the three DOF obtained either from the CSLDV or the fixed LDVs overlap closely. The normalized root mean square error between the displayed time-domain waveforms are 0.235 % for $V_z(t)$, 4.58%, for $\dot{\theta}_y(t)$ 3.42 %, and for $\dot{\theta}_x(t)$.

2.2.3 Sources of measurements errors and technical limitations of the CSLDV technique

The main practical limitation of CSLDV over conventional fixed LDVs is the greater influence of speckle noise as described in Section 1.2.

In particular, the amplitude of the speckle noise is known to increase with the scanning frequency Ω of the CSLDV beam [34, 42]. This effect is shown in Figure 11 where the scanning frequency changes from 40 Hz to 160 Hz with an increment of 40 Hz.

Another parameter influencing the speckle noise is the scan length. Speckle noise level increases as the spatial extent of the scan pattern increases since more speckle grains sweep

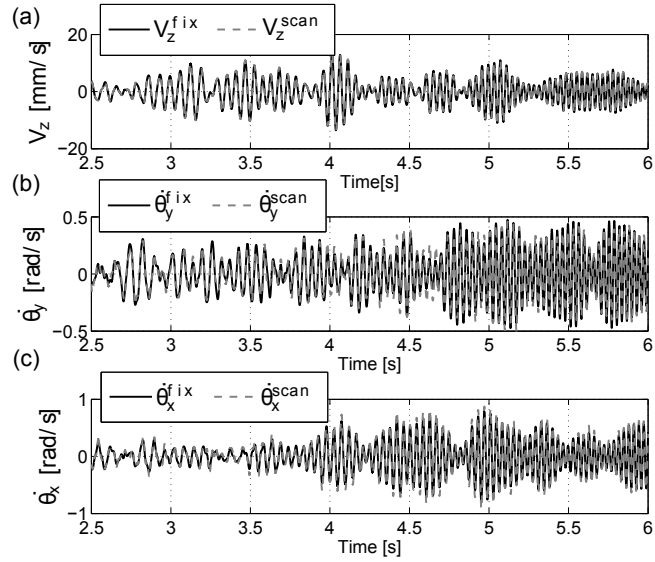


Figure 9: Comparison of the waveforms obtained using the CSLVD (indicated by the *scan* superscript) and the fixed LDVs (indicated by the *fix* superscript) for the three DOF of interest, as defined in Figure 5b. (a) $V_z(t)$, (b) $\dot{\theta}_y(t)$ and (c) $\dot{\theta}_x(t)$.

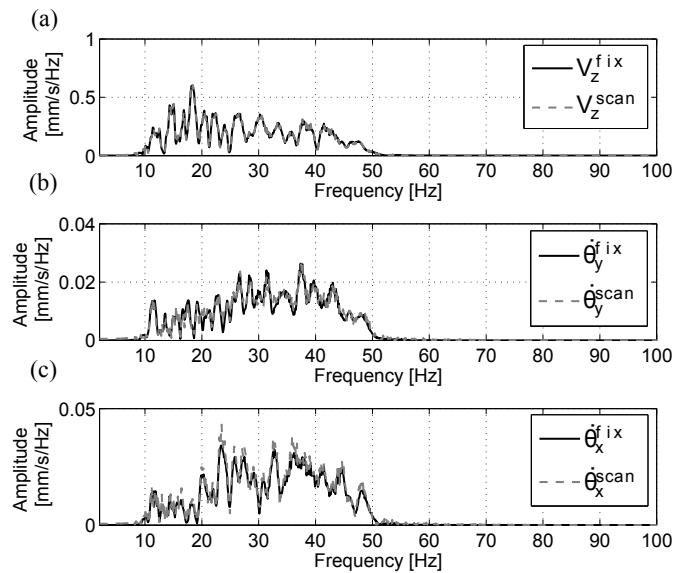


Figure 10: Same as Figure 9 but displaying instead the amplitude spectra of the three DOF defined on Figure 5b.

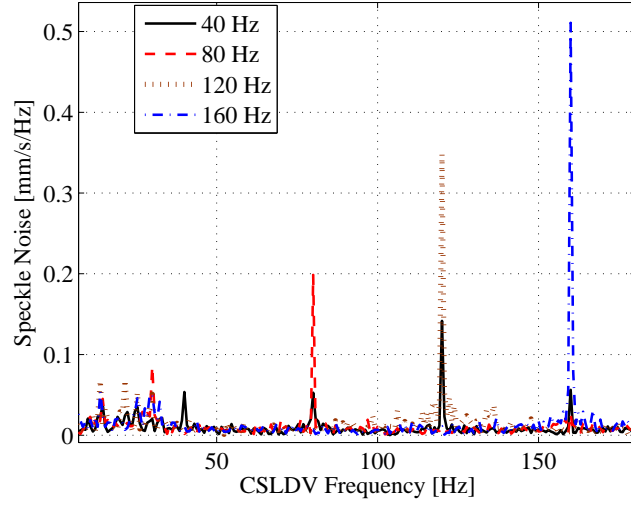


Figure 11: Effect of scanning frequency on the speckle noise.

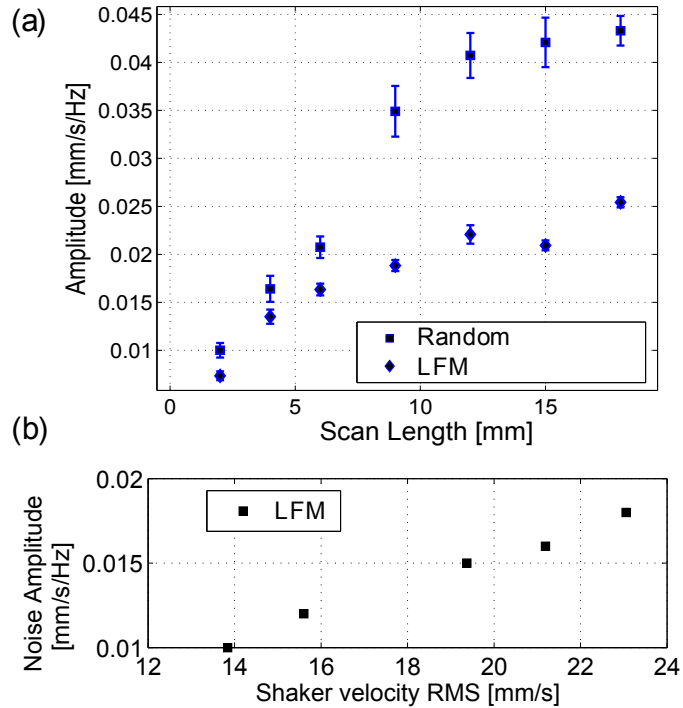


Figure 12: (a) Evolution of the mean noise amplitude measured in the frequency band $B_n=[80 \text{ Hz}-120 \text{ Hz}]$ (as defined in Figure 8) vs length of the linear scan covered by the laser beam. Both LFM and random shaker excitation were used in the same frequency band [10 Hz-50 Hz]. The distance between the tip of the shaker rod and the center O of the CSLDV scan was 10 cm. (b) Same as (a) but showing instead the influence of the root mean square amplitude of the shaker velocity on the measured noise amplitude for a 5 mm circular scan CSLDV.

through the laser beam [34, 42, 58]. To illustrate this effect, Figure 12a displays the evolution of the speckle noise amplitude computed over five successive measurements for increasing length of line scans from 5 to 20 mm. The speckle noise amplitude was estimated from the mean value of the frequency spectrum of the CSLDV signal $V(t)$ in the frequency band, B_n , [80 Hz to 120 Hz] where no translation or angular velocities amplitude is expected to be measured (e.g., see Figure 8). Two types of shaker excitation waveforms were used for this experiment: either an LFM waveform or a filtered white noise waveform (random signal) both in the frequency band [10 Hz to 50 Hz]. Speckle noise level increases as the scan length increases and it is more in case of random excitation as compared to LFM excitation. In practice, the amplitude of the test surface's vibrations needs to be sufficiently higher than the estimated speckle noise floor. However, this excitation amplitude can not be selected arbitrarily large, as it also drives the speckle noise amplitude by causing larger displacement of the test surface compared to the optical wavelength of the LDV (see Figure 12b obtained using a 5 mm circular scan).

$$Error = \frac{\int_{t1}^{t2} (V_z^{fix} - V_z^{scan})^2 dt}{\int_{t1}^{t2} (V_z^{fix})^2 dt} \quad (11)$$

Figure 13a displays the mean values of the normalized root-mean-square error computed by the Eq. (11) -over 10 measurements- of the gel's normal velocity V_z^{scan} estimated from the CSLDV with respect to the normal velocity V_z^{fix} given by the fixed LDVs which exhibit a linear increase with the scan length. Figure 13b displays the mean values of the normalized root-mean-square error -over 10 measurements- of the gel's angular velocity $\dot{\theta}_y^{scan}$ estimated from the CSLDV with respect to the normal velocity the gel's angular velocity $\dot{\theta}_y^{fix}$ given by the fixed LDVs.

In this case, the error for the angular velocity appears to decrease with the scan length $2R$ (for the selected range from 5 to 20 mm) as the CSLDV is actually sensitive to the product $R\dot{\theta}_y^{fix}$ and not $\dot{\theta}_y^{fix}$ [see Eq. (3)]. Thus increasing the scan length effectively enhances the amplitude of this term with respect to the background noise level. This effect is demonstrated in Figure 14 where the circular scan radius increases from 5 mm to 20 mm. Energy of the signal increases for the modulation part (angular vibrations) as the

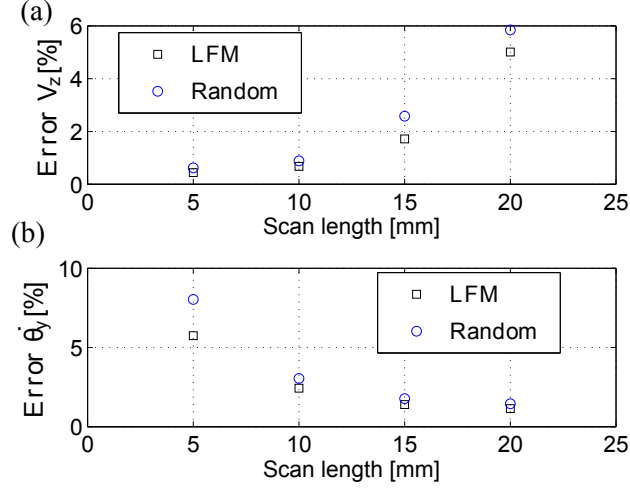


Figure 13: Evolution of the root-mean-square error of the CSLVD measurements with respect to the fixed LDV measurements of (a) normal velocity $V_z(t)$ and (b) angular velocity $\dot{\theta}_y(t)$ while the linear scan length of the CSLDV increases from 5 mm to 20 mm.

scan radius increases (see Figure 14b). However, one is limited to small value of R under the rigid body model's assumptions (see Figure 5).

Figure 15 shows the evolution of error for both normal and the angular vibrations vs shaker amplitude [given in RMS voltage] for a one cm long line scan. It shows that the error for the V_z and $\dot{\theta}_y^{fix}$ goes on decreasing with an increase in the shaker excitation amplitude. However, there is a trade off of the shaker excitation amplitude and the noise floor level which also increases proportionately.

Table 1: Variation of error vs the distance, L for a circular scan of 10 mm diameter.

Circular Scan 10 mm diameter			
L	$V_z^{fix} - V_z^{scan}$	$\dot{\theta}_y^{fix} - \dot{\theta}_y^{scan}$	$\dot{\theta}_x^{fix} - \dot{\theta}_x^{scan}$
mm	%	%	%
50	0.4276	3.226	2.002
60	0.4723	3.314	2.056
70	0.4783	3.165	2.093
80	0.6598	3.680	2.431
90	0.6509	4.128	2.481
100	0.5933	5.098	3.347
110	0.7013	6.465	4.652
120	0.7781	7.217	5.197

Table 1 shows the variation of errors between the three DOF obtained from the fixed

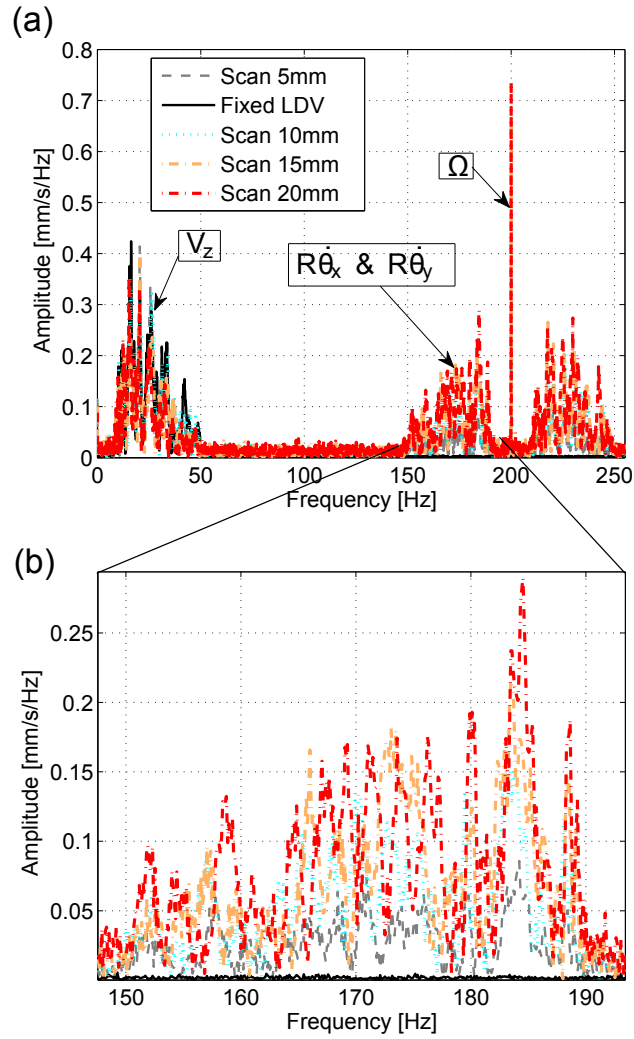


Figure 14: (a) Effect of increasing the scan radius from 5 mm to 20 mm of the circular CSLDV on the modulation signal energy. (b) Closeup view of the modulation signal energy in the frequency band of [150 Hz-190 Hz] which contains the information of angular vibrations.

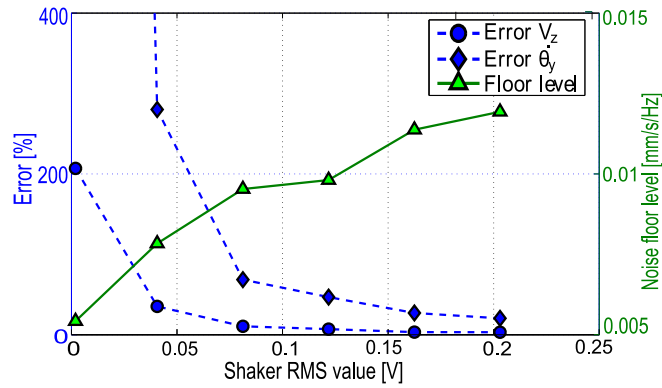


Figure 15: Error for both normal and the angular vibrations decreases as the shaker amplitude increases but it increases the noise floor level.

LDVs and the CSLDV for a 10 mm circular scan diameter. It is clear from the table that as the distance L increases, the error for both translational and angular vibrations increases. This increase in error is due to the low SNR since the wave energy reduces as the distance L increases at a given excitation amplitude.

2.3 Applications to hand tremor sensing

Tremor is defined as an involuntary, rhythmic oscillatory movement of a body part [57] (e.g., hand shaking). Pathological tremor is the most common movement disorder (e.g., as occurring during Parkinson syndrome). Tremor can also occur when the affected body part maintains position against gravity (e.g., extending arms in front of body) or from muscle contraction against stationary objects (e.g., holding a heavy object in one hand for a long time). The tremor has typically a frequency of 4–12 Hz, and its amplitude increases with anxiety or fatigue and at the very end of goal-directed movements. Measuring tremor-induced vibrations of a specific joint along multiple DOF using a non-contact CSLDV could potentially be useful for physiological studies or haptic applications[44]. As a proof of concept, the CLSDV methodology discussed in Section 2.1 and 2.2 is applied here for measuring both translation and angular velocities resulting from hand tremor of a healthy male subject (25 yr old) with no known neuromuscular disorders.

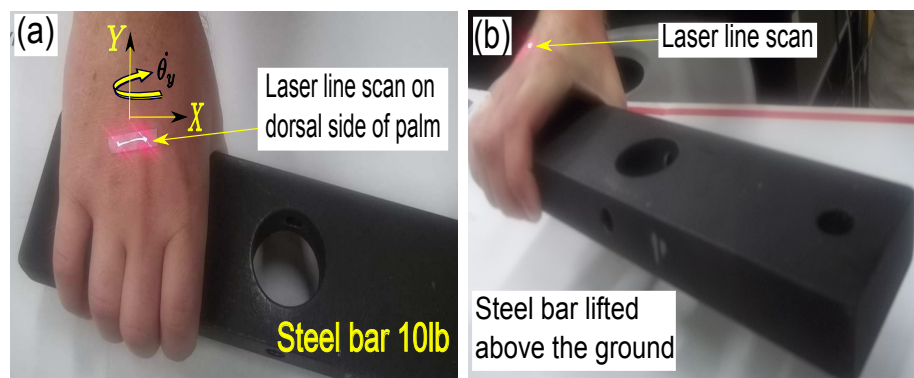


Figure 16: (a) Top view snapshot of the experimental setup. The subject is holding horizontally a 10 lb steel bar from its extremity. The CSLDV performs a 10 mm line scan to measure the normal velocity $V_z(t)$ and the angular velocity $\dot{\theta}_y(t)$ resulting from hand tremor. (b) Isometric view of the setup.

To do so, the CSLDV beam scans along a 10 mm line on the dorsal side of the palm while

the subject is holding the end of 10 lb steel bar (see Figure 16). The Cartesian coordinates system associated with the line scan is shown on Figure 16a. Two fixed LDV beams are positioned at the end of the short line scan for validation purposes as shown on Figure 5a. The same experimental setup shown in Figure 6 and described in Section 2.2 is used here to control and orient the fixed and scanning LDV beams. In this configuration the translational velocity $V_z(t)$ primarily corresponds to the up and down motion of the hand while the angular velocity $\dot{\theta}_y(t)$ primarily results from the wrist rotation. Figures 17 and 18 show the close overlap of the time-domain signals (after filtering in the frequency band [5 Hz to 50 Hz]) and the corresponding frequency amplitude spectra for the two DOF of interest $V_z(t)$ and $\dot{\theta}_y(t)$.

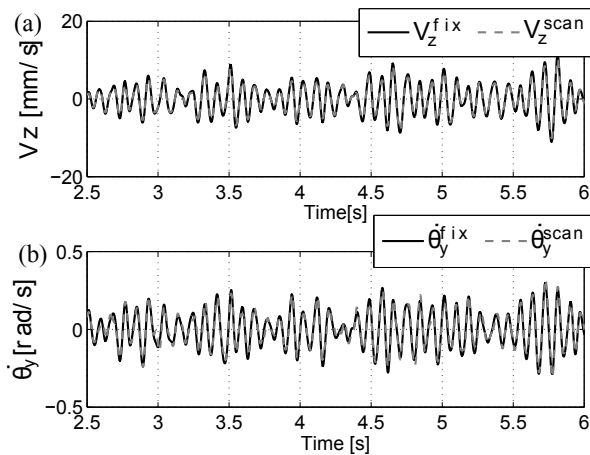


Figure 17: Comparison of the waveforms obtained using the CSLVD (indicated by the *scan* superscript) and the fixed LDVs (indicated by the *fix* superscript) for the two DOF of interest, as defined in Figure 16. (a) $V_z(t)$ and (b) $\dot{\theta}_y(t)$.

The normalized root mean square error between the displayed time-domain waveforms are 1.6 % for $V_z(t)$, and 4.5 % for $\dot{\theta}_y(t)$. These results further validate the proposed CLSDV methodology. Furthermore, it can be noted that the amplitude spectra of both DOF exhibit the same dominant frequency peak around 11 Hz; this results from the hand tremor of the subject because he was performing a sustained and fatiguing task [38].

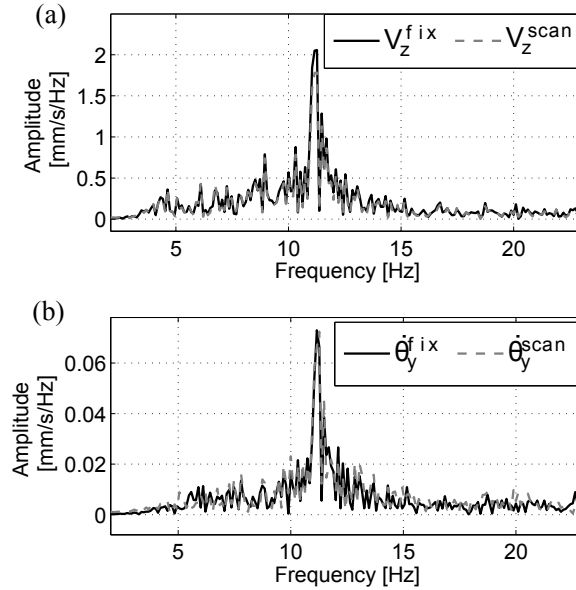


Figure 18: Same as Figure 17 but displaying instead the amplitude spectra of the two DOF defined on Figure 16.

2.4 Summary and conclusions

A Laser Doppler Vibrometer (LDV) offers a non-contact alternative to conventional skin-mounted sensors (e.g., accelerometers) for measuring natural human body vibrations at specific joints or over limbs. Indeed, LDV may be the only practical alternative for measuring multiple DOF over very small human body parts (e.g., fingers, tendons, small muscles) onto which conventional vibration sensors can not be skin-mounted easily. Indeed these skin-mounted sensors have a finite size typically larger than a focused laser beam, and these sensors may cause measurements artifacts such as added mass or tethering problems. Furthermore, the CSLDV technique provides a means for measuring multiple DOF of a vibrating surface using a single scanning laser beam.

This study used the CSLDV technique for measuring random broadband vibrations with low frequency content (i.e., $f < 100$ Hz here) –such as natural vibrations of skeletal muscles during voluntary contractions– using a high scanning frequency (of 200 Hz) of the laser beam over the test surface. The proposed approach was validated using small line and circular scan patterns of the laser beam to measure both translational and up to two

angular velocities of gel samples mimicking human soft tissues. Additionally, this study demonstrated the feasibility of the proposed methodology for measuring the translational and angular velocity resulting from natural hand tremor of a human subject lifting a heavy steel bar. These results indicate that this CSLDV technique could be used to provide non-contact motion sensing for various applications relying on sensing fine motor control such as telesurgery or haptic technology.

CHAPTER III

LONG SCAN

A long scan CSLDV technique is used to extract the measurements of normal velocity vibrations from multiple locations. Previous studies [48, 4] have used accelerometers to measure vibrations of human skeletal muscles. The main problems with the use of accelerometers or other contact sensors are the mass loading effects, tethering problems, cable dynamics and long setup time requirement. These limitations are overcome using the non-contact way of CSLDV sensing technique. It is very easy to use this CSLDV technique which gives multiple locations measurements by a single LDV sensor steered by a mirror. The goal of this chapter is to first validate this technique on a custom made gel (mimicking human body soft tissue) and then implement (Chapter IV) it for getting the dynamic elastography Imaging of human skeletal muscles using external vibrating source.

3.1 Methodology: demultiplexing the CSLDV signal

The Nyquist sampling theorem [55] states that a bandlimited analog signal can be perfectly reconstructed from an infinite sequence of samples if the sampling rate (or sampling frequency) exceeds $2f_{max}$ samples per second, where f_{max} is the highest frequency of the original signal [55]. In this study, the bandlimited signals of interest are the vibrations measured by the CSLDV along its periodic scanning trajectory-denoted $\vec{r}(t)$ - over the vibrating surface. The scan period T is defined as the smallest time-interval required by the laser beam to trace the closed scan trajectory back to where it initially started one time. One simple periodic scanning trajectory used in this study hereafter is a harmonic linear scan or line scan such that

$$\vec{r}(t) = L \cos(2\pi\Omega t)\vec{e} \quad (12)$$

where $2L$ is the scanned length and the unit vector \vec{e} specifies the spatial orientation

of the linear scan along the vibrating surface (see Figure 19a). $\Omega = 1/T$ represents here the scanning frequency of the CSLDV's optical beam. If the scanning frequency Ω exceeds $2f_{max}$, then the measured velocity signal by the CSLDV can be demultiplexed to simultaneously extract the projection of the surface velocity vectors onto the laser beam direction over the whole scan length [60, 1, 11]. This demultiplexing operation is analogous to telecommunication applications where multiple analog signals originally combined into one single broadcast signal (also referred to as time-division multiplexing) need to be sorted out at the receiver's end. More generally, the various types of periodic scan geometry or patterns described in the previous literature[67] (e.g., two-dimensional patterns such as Lissajous curves) can also be used to extract synchronized vibration measurements at multiple locations using a single CSLDV. In this case, the scan duration T should also be selected such that $T < 1/(2f_{max})$.

The sampling frequency of the velocity signal $V(t)$ measured by the CSLDV is denoted by f_s hereafter. For the sake of simplicity, it is assumed here that scan duration T over the test surface is an exact multiple of $1/f_s$ following the formalism developed in previous studies [60, 1, 11]. Hence, the maximum number N of stationary virtual receivers that can be created along the scan trajectory after demultiplexing is

$$N = Tf_s \quad (13)$$

Note that the effective sampling frequency of the N virtual velocity signals $\tilde{V}_j(t)$ ($j = 1..N$) extracted from the original CSLDV velocity output $V(t)$ after demultiplexing is reduced to $1/T$. Assuming that the laser beam is over the reference location $\vec{r}(t_{ref})$ (e.g., extreme end A of the scan line on Figure 19) at the reference time t_{ref} , then the discrete locations \vec{r}_j of the N stationary virtual receivers along the scan trajectory are given by[60, 1, 11]

$$\vec{r}_j = \vec{r}(t_j), \text{ for } j = 1..N \quad (14)$$

where the discrete times t_j are determined by the sampling frequency f_s such that

$$t_j = t_{ref} + \frac{(j-1)}{f_s}, \text{ for } j = 1..N \quad (15)$$

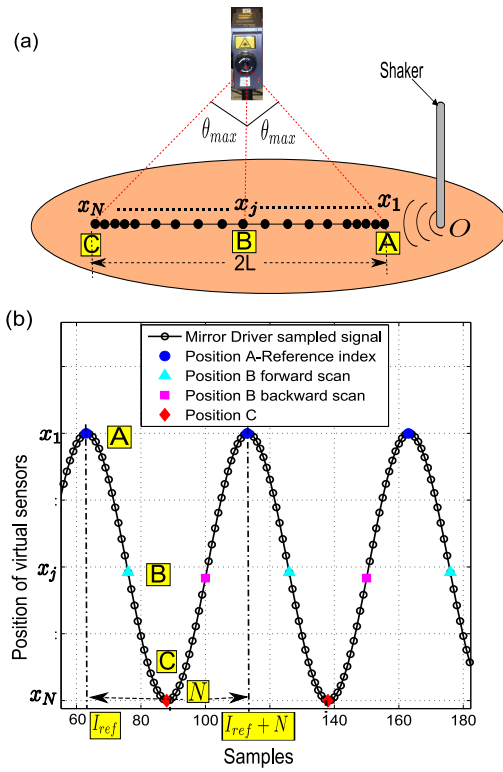


Figure 19: (a) Schematic of the proposed CSLDV methodology using a linear scan of extent $2L$. The three locations marked A-B-C correspond to the middle point and end points of the linear scan. The angle noted θ_{max} corresponds the maximal angular deflection of the continuously scanning laser beam. Dot symbols indicate the locations of the N virtual sensors x_j ($j=1\dots N$) assuming that a sinusoidal waveform is used to steer the laser beam over the test surface. (b) Discrete representation of the periodic sinusoidal waveform used to steer the laser beam. Note that a uniform temporal discretization of this waveform (along the horizontal axis) results in a non-uniformly spaced linear array of the effective locations of the N virtual sensors (vertical axis) along the test surface as shown in (a).

The same discrete times t_j are used to demultiplex the corresponding N virtual velocity signals $\tilde{V}_j(t)$ from the original CSLDV velocity output $V(t)$. Using discrete notations, the n^{th} sample of each virtual velocity signals $\tilde{V}_j[n]$ (discretized at the effective sampling frequency of $1/T$) obtained from demultiplexing of the CSLDV's signal are [60, 1, 11]:

$$\tilde{V}_j[n] = V[I_{ref} + (n - 1)N + (j - 1)], \text{ for } j = 1..N \quad (16)$$

where I_{ref} is the discrete index (i.e., sample number) corresponding to the reference time t_{ref} for the discretized CSLDV's signal V . In Eq. (16), brackets notations are used to refer to the discretized version of the velocity waveforms $\tilde{V}_j(t)$ and $V(t)$. Figure 19a shows a schematic of the positions of the virtual sensors $\vec{r}_j = (x_j, 0, 0)$ [see Eq. (14)] for the case of a linear harmonic scan [see Eq. (12)] which will be used in the remainder of this chapter. The positions x_j are determined by the angular deflection of the CSLDV's optical beam oscillating at the scanning frequency Ω (see Figure 19b). Note that the virtual sensors (at positions x_j , $j = 1..N$) are not equally spaced due to the combined influence of the sinusoidal waveform used for scanning the laser beam and the actual inertia of the steering mirror. The spacing of the virtual sensors is larger next to the middle point B as compared to the end points A and C.

3.2 Experimental validation

3.2.1 Experimental setup

A description of the experimental setup shown on Figure 20a is given hereafter. A gel sample, made from commercially available gelatin with a stiffness (Young's modulus) of approximately 13 kPa, (mimicking human body soft tissues), is excited by an electrodynamic mini-shaker (B & K Model 4810). A 50 mm by 3 mm thin rectangular-shaped piece of retro-reflective tape (3MTM ScotchliteTM - 9810 multipurpose tape) is applied onto the gel surface (see Figure 20b) as this gel medium is very transparent and diffusive which makes it a poor reflector of the laser beam. The LDV (PolytecTM Model PDV 100) labeled as CSLDV on Figure 20a is used to continuously scan the gel surface along the retro-reflective tape. The CSLDV's beam is deflected using a two-axes fast steering mirror (1/2 inch diameter, maximum angular deflection of 2.86° or 50mrad in closed feedback control loop),

mounted on piezoelectric actuators (PhysikTM InstrumenteTM Model S-334). For all the experimental results presented hereafter, the scanning frequency of this mirror is set to $\Omega = 200$ Hz, which is well below the first resonance frequency of the oscillating mirror (≈ 1 kHz) to optimize the angular precision of the fast scanning mirror.

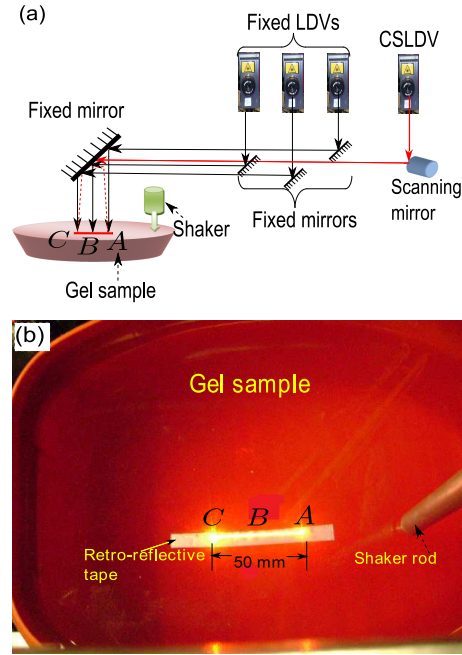


Figure 20: (a) Schematic of the experimental setup (b) Top view of the gel's surface.

Finally, the linear scan pattern of this CSLDV is reflected onto the horizontal gel surface using a fixed mirror-mounted at a 45° angle to achieve normal incidence. The three other LDVs are used to measure the actual gel's vibrations at three fixed points -labeled as A, B and C on Figure 19 and Figure 20- which correspond to the two extremities and middle of the linear scan trajectory. The velocity measurements of these so-called fixed LDVs are used to validate the measurements of three of the virtual sensors extracted from the CSLDV signal after demultiplexing, and whose locations coincide with points A-C on the gel. All fixed and scanning LDVs as well as reflective mirrors were mounted on an optical table (Newport Model RS2000-46-8) supported by pneumatic Stabilizer Isolators (Newport Model S-2000 series). The shaker was mounted on a separate fixed table so that parasitic vibrations could not contaminate the LDV's measurements. A low pass filter of 1 kHz was applied internally by each PDV 100 vibrometers to the measured velocity signal (with a sensitivity of 125

mm/s/V). The same data acquisition board (National InstrumentsTM Model cDAQ-9178) was used to simultaneously sample all four LDVs' signals with a sampling rate of $f_s = 10$ kHz.

3.2.2 Influence of speckle noise on the CSLDV signal

Speckle noise as described in Section 1.2 limits the accuracy of the CSLDV technique. In order to overcome this limitation, one of the parameters, among others, is the amplitude of the test surface's vibrations. This excitation amplitude needs to be, in practice, sufficiently higher than the estimated speckle noise floor. However, there is a limitation on the excitation amplitude as explained in Section 2.2.3. Figure 21 displays the power spectrum of the velocity signal- before demultiplexing- measured using both the fixed LDV B and the CSLDV with or without (i.e., baseline conditions) shaker excitation of the gel surface. The power spectra are displayed with a 5 Hz resolution along the frequency axis. The raw velocity measurements were collected using the setup shown in Figure 20 with a 50 mm long linear scan. The shaker excitation was a 7 s long linear frequency modulated (LFM) waveform [29] ranging from 10 Hz to 50 Hz. The noise floor level, primarily due to the speckle noise effect, was estimated here from the mean value of the power spectrum in the frequency band $B_n = [80 \text{ Hz to } 120 \text{ Hz}]$ (as shown on Figure 21 and discussed further in appendix B.2), i.e., just above the [10 Hz to 50 Hz] frequency band excited by the shaker. Furthermore, Figure 22 shows a nearly linear increase of the noise floor level with the length of the linear scan up to 60 mm (the first value at zero mm corresponds to the fixed LDV measurements). This primarily occurs because more speckle grains sweep through the laser beam as the spatial extent of the scan pattern increases [42]. Figure 22 shows that the signal amplitude is nearly two orders of magnitude (factor of about 100 as compared with the signal in Figure 21) larger than the noise floor level for the selected setup and thus does not significantly affect the CSLDV measurements here for the scan length up to 60 mm. Thus these results indicate that the speckle noise is not a significant nuisance here given the selected experimental setup and parameters (see Figure 20) .

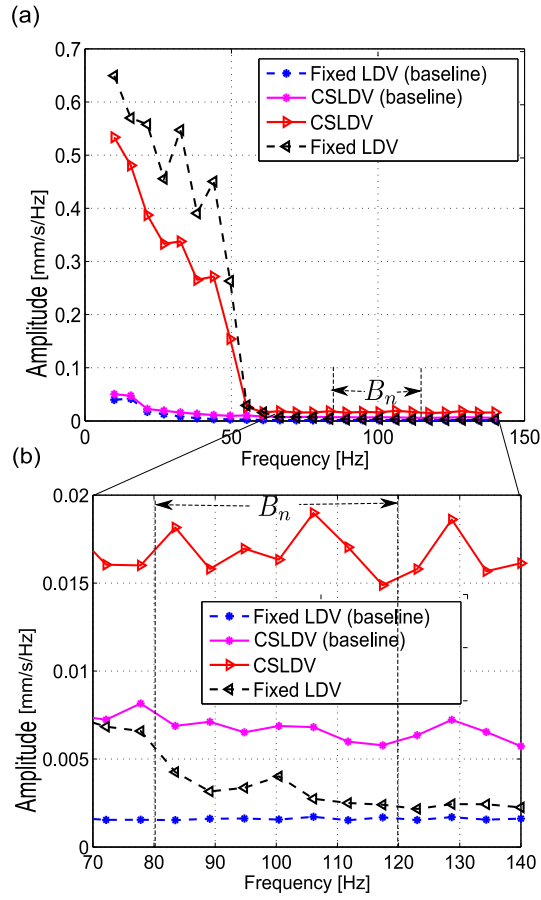


Figure 21: Comparison of the amplitude spectra of the velocity signal- before demultiplexing- measured using both the fixed LDV pointing above location B (see Figure 20b) and the CSLDV with or without (i.e., baseline condition) shaker excitation of the gel surface. The scan length is 50 mm. (b) Close-up view of the noise floor level of the same four power spectra shown in (a) around the frequency band $B_n = [80 \text{ Hz to } 120 \text{ Hz}]$.

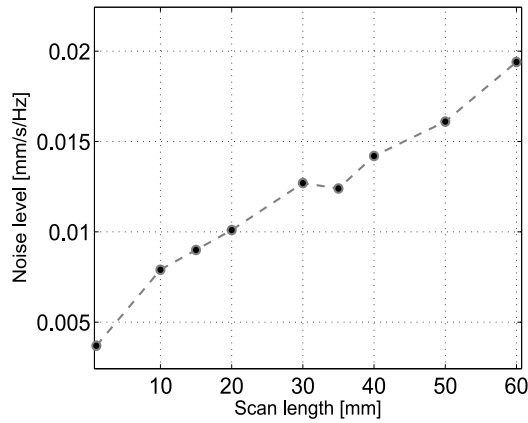


Figure 22: Variation of the average noise level in the frequency band B_n [80 Hz to 120 Hz] vs the length ($2L$) of the linear scan along the gel surface.

3.2.3 Comparison between fixed LDV and CSLDV measurements at the same location

The three panels in Figure 23a-c display the same time-interval of three demultiplexed velocity waveforms (plain line) corresponding to virtual sensor located closest to the three locations A-C (as indicated on Figure 19a and Figure 20b) using the appropriate indexing of the CSLDV signal following Eq. (16) i.e., here $j = 1, N/4$ and $N/2$ (see Figure 19b). The gel surface was excited with the same 7 s long LFM waveform (from 10 Hz to 50 Hz) used in the previous Section 3.2.2. In order to validate these CSLDV measurements, the waveforms obtained from the three fixed LDV beams pointing over the same three locations A-C were also demultiplexed (or downsampled) following the exact same indexing sequences used for the CSLDV signal corresponding to locations A-C over the 50 mm linear scan. These three demultiplexed waveforms obtained for each fixed LDVs are also displayed on Figure 23a-c as dashed lines (very close overlap). The normalized root mean square error between the demultiplexed waveforms measured with the fixed or scanning LDVs are respectively 1.2 %, 3.2 % and 2.2 % for locations A, B and C. Furthermore, Figure 24 compares in a similar pairwise fashion the amplitude spectra of the waveforms corresponding to locations A, B and C. Similar low error values were obtained ($< 4\%$) for all tested scan length up to 60 mm using the same experimental setup. Overall, these results indicate that the velocity measurements obtained either from the CSLDV after demultiplexing or the fixed LDVs overlap closely for the selected experimental setup.

3.2.4 Matched filtering of virtual sensors from CSLDV

The CSLDV technique used to measure the vibrations emanating from the shaker's tip and propagating towards the other end of the tape along a 5 cm long linear scan. Using the methodology developed in Section 3.1, the CSLDV signal was further demultiplexed to create a line array of $N = 50$ virtual sensors along the linear scan. Note that for the selected linear scan [see Eq. (12)], the virtual sensors (at positions $x_j, j = 1..N$) are not equally spaced along the tape axis due to the selected sinusoidal voltage signal used for steering the scanning mirror (see Figure 20b). As a result, the virtual sensors appear squeezed together

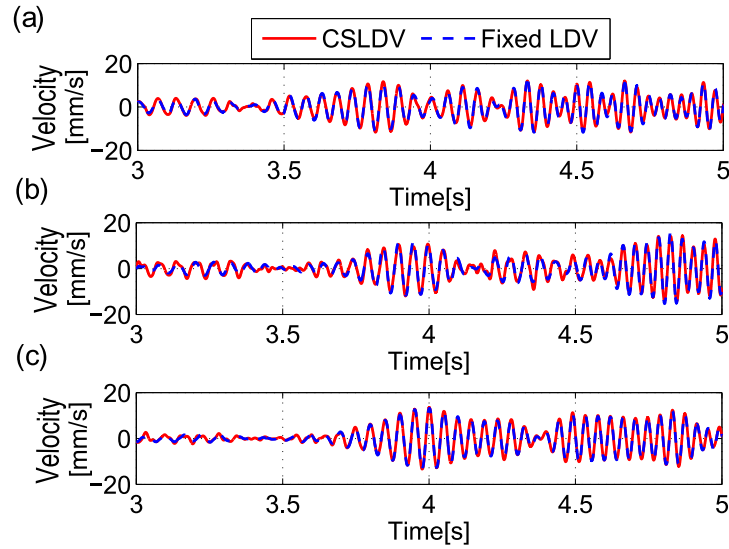


Figure 23: Comparison of the waveforms recorded by the fixed LDVs to the corresponding virtual sensor's waveform, obtained after demultiplexing of the CSLDV signal, at the same specific locations A, B and C along the 50 mm linear scan.

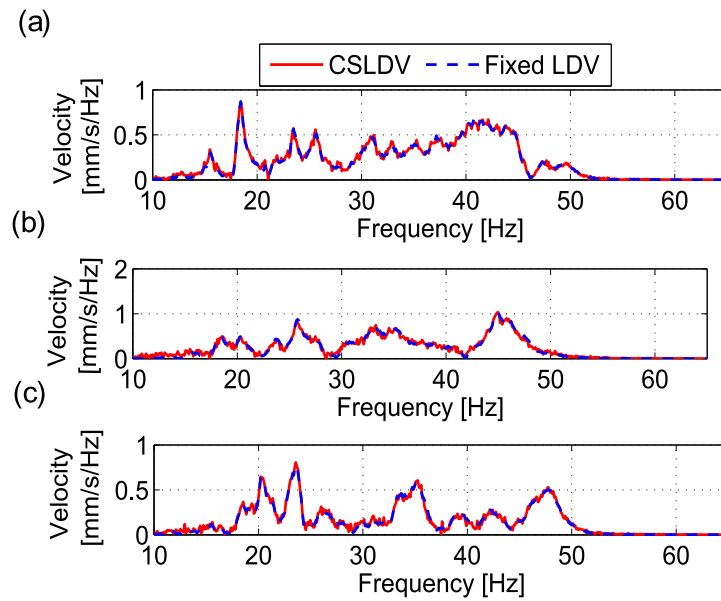


Figure 24: Same as in Figure 23 but displaying instead the corresponding amplitude spectra each waveform over locations A-C.

near the ending positions A and C where the scanning mirror (and hence laser beam) moves the slowest when compared the larger spacing of virtual sensors close to middle position B, where the laser beam moves the fastest. Furthermore, the laser beam actually goes back and forth along the same scan line respectively from points A to C and then from points C to A (see Figure 20b). Hence the demultiplexed waveforms obtained from the first

25 virtual sensors closely overlap with the last 25 of the virtual sensors (taken in reverse order). In order to measure the effective arrival time of the shaker's signal at each of the $N = 50$ virtual sensor locations, the demultiplexed waveforms $\tilde{V}_j(t)$ extracted from the original CLSDV signal [see Eq. (16)] were each matched-filtered (i.e., cross-correlated) with a downsampled replica at 200 Hz of the original LFM waveform (sampled at $f_s = 10$ kHz and synchronized with the original CLSDV signal). Note that in order to maintain consistency of the timing reference between all virtual sensors- as required by the matched-filtering operation [69, 29, 26]- the replica waveform used for the j^{th} virtual sensor was time-shifted by a delay $(j-1)/f_s$, ($j = 1..N$), compared to the replica waveform used for the first virtual sensor (at location A here). This time-shifting operation allows compensation for the fact that the laser beam does not move instantaneously from position x_1 (i.e., position A) to position x_j during each scan period but instead takes a finite duration $(j-1)/f_s$ based on Eqs. (13) to (15).

Figure 25 shows the $N = 50$ stacked demultiplexed waveforms after matched-filtering with the time-shifted and downsampled LFM replica. Figure 25 shows that the CLSDV can clearly track a propagating pulse primarily associated with a low-frequency flexural wave emanating from the shaker location and propagating towards the far end of the tape mounted on the gel. Besides, no significant reflected pulse is observed from the end of the gel container, likely due to the high mechanical damping of the gel medium. The peak amplitude of each pulse is marked on Figure 25a respectively by lozenges and square symbols whether the laser beam actually moves from extremities A to C or C to A. The small mismatch between the waveforms measured from A to C or C to A is primarily due to small errors in the scanning mirror's positioning -especially when its scanning velocity is maximal next to point B- as well as fluctuations of the gel surface. As expected, the propagation velocity of this pulse appears to be nearly constant since the linear scan area overlays a very homogeneous gel medium. Thus, the average phase velocity of this propagating pulse can be readily estimated from the slope of the linear interpolation fitting the peak amplitudes and corresponding arrival times [13]. Given the relatively small frequency bandwidth used in this study, dispersive effects on the measured phase velocity were neglected here. Finally, for

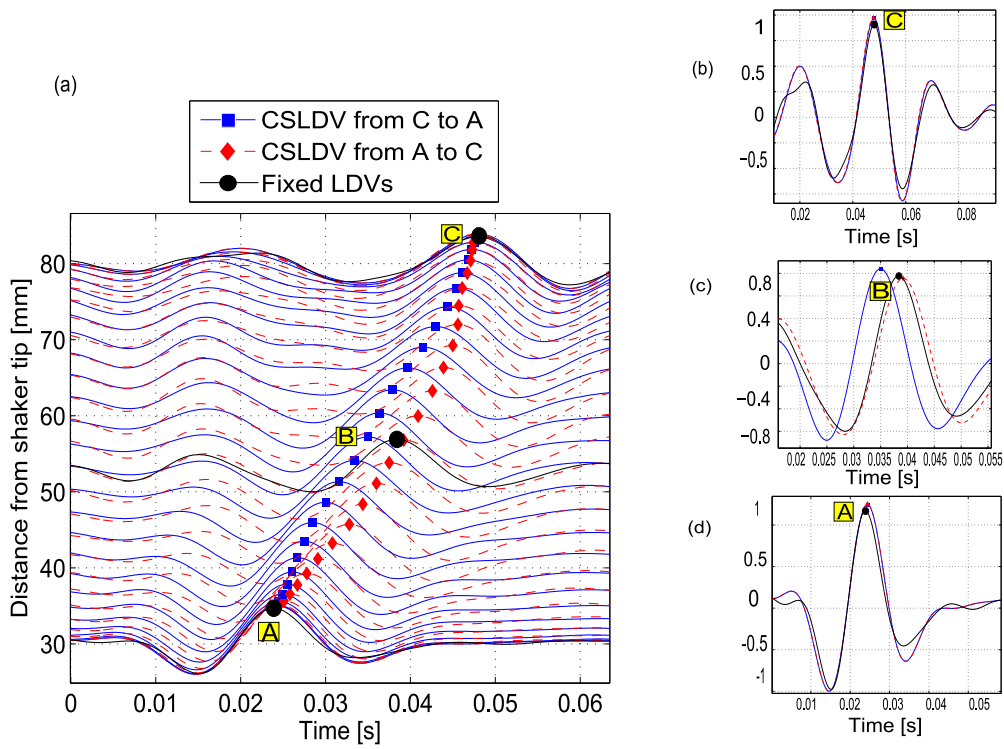


Figure 25: (a) Stacked demultiplexed CSLDV waveforms of the gel obtained after matched-filtering with a time-shifted and downsampled replica of the shaker LFM excitation. The vertical axis indicates the distance of each of the virtual sensors from the shaker's tip. (b-d) Comparison of three selected demultiplexed waveforms using the CSLDV associated with positions A-C to the corresponding waveforms obtained using a fixed LDV pointing above the same positions A-C.

comparison, the matched-filtered waveforms obtained using the three fixed LDVs positioned over locations A, B, C are also displayed on Figure 25a and their peak amplitude are marked by large circles. Additionally, Figure 25b-d show close up views of individual measurements obtained from the three fixed LDVs and the corresponding virtual sensors whose locations are closest to the reference points A, B and C on the gel. Overall, Figure 25 confirms the close agreement between the average propagation velocity c estimated either using the line array of virtual sensors ($c=1.99\text{m/s}$) or the three fixed LDV ($c=2.06\text{m/s}$). The shear wave velocity can be found by the relationship $c_t = c_r/0.96$ [31] and using Eq. (17) [56] the Young's modulus of the gel is ≈ 13 kPa.

$$E = 3\rho(c_t)^2 \quad (17)$$

3.3 Difference of phase velocities

Two different approaches for finding the phase velocity of the propagating waves on the gel surface are shown in Figure 26. In first approach, the phase velocity is obtained from the slope of the line joining the array of virtual sensors obtained from the cross-correlation function of the demultiplexed CSLDV signals and the shaker output signal down-sampled for position A. This approach is shown as case-1 in Figure 26. It is clear from the plot that there is a certain initial time delay after which the direct wave arrivals, obtained from the normalized cross-correlation (see Figure 25b,c and d), start appearing. This delay is because the shaker output signal, demultiplexed for position A, does not exactly synchronize with the demultiplexed CSLDV signal for position A. In order to see the line joining the array of virtual sensors, starting from the origin, another approach of finding the cross-correlation function is used as shown in Figure 26 as case-2. This approach uses the cross-correlation function between the demultiplexed CSLDV signal and the demultiplexed CSLDV signal for position A to see the direct wave arrivals. In case-2, the line joining the direct wave arrivals (normalized cross-correlation functions) starts from the origin. There is no initial time delay in this case-2, which is because the demultiplexed CSLDV for position A first cross-correlates itself and then with the other demultiplexed CSLDV time domain signals.

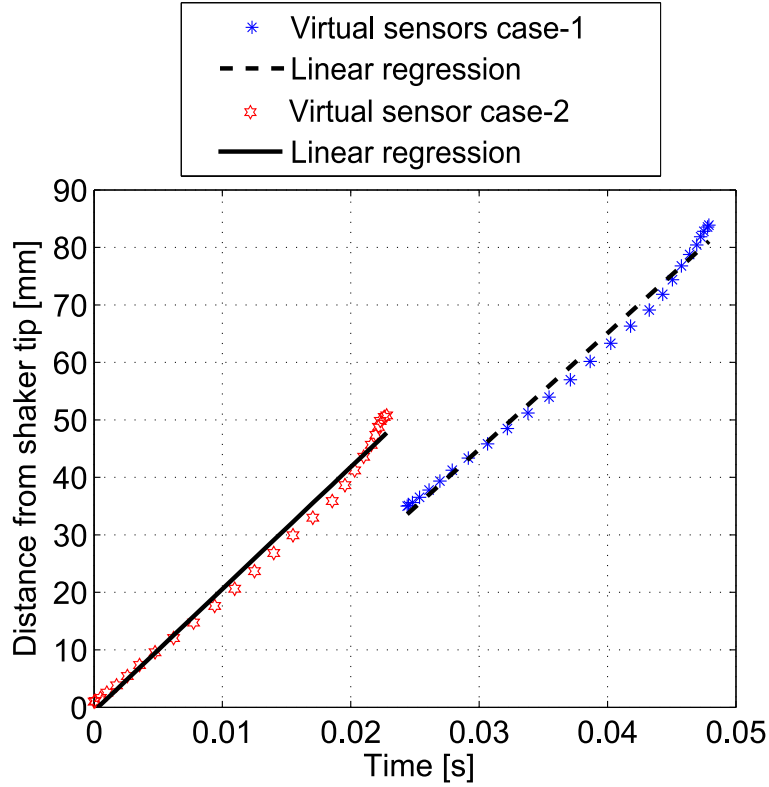


Figure 26: Difference of phase velocities using two different approaches. (a) Phase velocity obtained in case-1 from the slope of the line joining the array of virtual sensors obtained from cross-correlation function of the demultiplexed CSLDV and the shaker output signal down-sampled for position A. (b) Case-2 is same as case-1 but the cross-correlation function is between the demultiplexed CSLDV and the demultiplexed CSLDV for position A.

Phase velocities obtained from case-1 and case-2 are 1.99 m/s and 2.09 m/s respectively. This study follows the approach of case-1.

3.4 Summary and conclusions

This chapter uses a CSLDV to extract synchronized broadband vibrations measurements at multiple locations using a single laser beam rapidly scanning the test surface. The proposed approach was validated using linear scans- up to 5 cm long -on gel samples (mimicking human soft tissues) for low frequency vibrations ($f < 100$ Hz). The spatial extent of the scan pattern was limited by the maximal angular deflection of the fast scanning mirror used to steer the laser beam. Furthermore, the highest frequency of the surface vibration which can be accurately extracted from the CSLDV signal (i.e., $f = 100$ Hz in this study) using the proposed demultiplexing algorithm is limited by the scanning frequency of the laser

beam tracing the scan pattern (set to 200 Hz in this study). The ability to measure surface vibrations at higher frequencies over larger areas could potentially be enhanced by using a different technology to steer the laser beam faster and over wider extent. However, in practice, increasing either the scanning frequency of the laser beam or the scan dimensions both increase the amplitude of the speckle noise: this may eventually limit the accuracy of the CSLDV measurements if the scan dimensions or scan frequency become excessively high. Finally, the results of this study demonstrate the applicability of the proposed CLSDV methodology for measuring the velocity of a low-frequency flexural wave propagating along the gel surface.

CHAPTER IV

ELASTOGRAPHY

The stiffness of skeletal muscles has been proved to be a very important property which keeps the muscle functions appropriately. The stiffness of skeletal muscles vary, among others, with their physiological state such as maximum contraction level (MVC) and fatiguing task. Muscle becomes stiffer during contraction at different levels of MVC and in some pathological condition such as spasm, cramps, oedema and delayed onset muscle soreness[20]. Muscle stiffness contribute significantly to its performance in eccentric, isometric, and concentric activities[72]. Therefore, it is important to assess muscle stiffness quantitatively to understand its proper functionality. A number of the methods have been developed to find the muscle stiffness quantitatively. These methods include indentation method [77], Sonoelastography [33], transient elastography [13, 20, 54], supersonic shear imaging [53, 52], shearwave dispersion ultrasound vibrometry [70]and the magnetic resonance elastography [7]. These studies have unique features and limitations for their in vivo studies. One of the limitations is their inability for finding the stiffness of musculotendinous areas or when the skeletal muscles are at high intensity contraction level of MVC. The long line CSLDV techniques as discussed in Chapter 3 present a new method with its application to skeletal muscle muscle vibration measurements and overcome the aforementioned limitation.

4.1 Dynamic elastography

Dynamic elastography is a stiffness imaging technique that uses an external source of vibration such as ultrasound elastography. There are some challenges in ultrasound elastography, one of which is its inability to image human body soft tissues at their superficial levels. Ultrasound requires an additional matching layer of gel between the ultrasound probe and the human body surface in order to obtain images of superficial layers. This issue has been addressed by this novel CSLDV technique, in which the wave velocity field is mapped over

the skeletal muscle surface. For instance, when a shaker excites human biceps, it produces waves on the biceps' surface. Normal vibrations are measured by the fast long line CSLDV, and, using the matched filtering (cross-correlation functions) technique, the time delays of direct arrivals at each virtual sensor give the slope of the surface wave velocity, c_r . The stiffness of the biceps is found using the Eq. (17), where E is the material elastic stiffness, ρ is the density of muscle which is approximately $1000 [kg/m^3]$ [20] and c_t is shear velocity.

The objective of this chapter is to measure the stiffness of human biceps muscle at different contraction levels of MVC using the CSLDV technique. An external source of vibration will be used to generate flexural waves over the biceps. A fixture will be designed for measuring the biceps' contraction force. The stiffness changes of biceps brachii with respect to different physiological states (e.g., different wrist position and elbow joint angles) will be presented in detail in this chapter.

4.2 Experimental setup

4.2.1 Design of the fixture for biceps contraction setup

Figure 27a shows a 3D CAD model of the fixture design for the biceps contraction setup. It shows a rigid steel structure mounted on a heavy table. There is a force transducer (load cell) attached with the steel bars, which measures the biceps pull force. On the other end of the table, a shaker is attached with X-Y linear stages, and the shaker rod can be moved up and down in the z-direction in order to adjust for big and small biceps [see Figure 27b]. Figure 27c shows the finite element analysis, performed for the steel structure, which has been simulated for the maximum pulling force applied by the biceps with a factor of safety 5, which is 500 N. It is clear that the maximum Von-Mises stress (42 MPa) in the steel structure is well below its yield stress (i.e., 250 MPa).

4.2.2 Complete experimental setup

The schematic of the experimental setup shown in Figure 28a. The set of equipment includes four fixed LDVs (Polytec PDV 100, max. bandwidth 22 kHz). One of the fixed LDVs is made the CSLDV when it strikes the fast scanning mirror, while three other LDVs are used for its validation. A fast scanning mirror (PhysikTM InstrumenteTM, Model S-334)

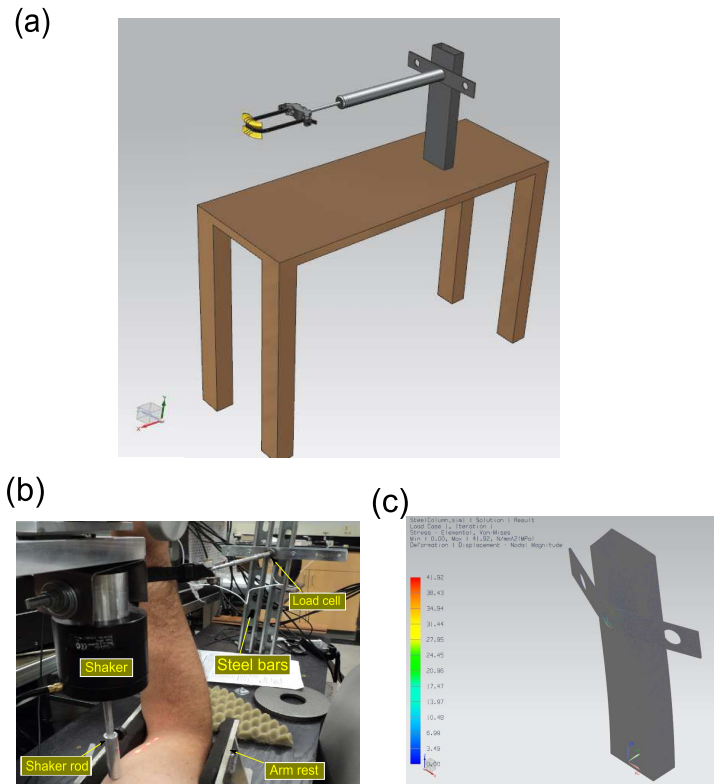


Figure 27: 3D CAD model of the fixture used to measure the force of biceps contraction. (b) Snapshot of the experimental setup with the biceps fixture and the shaker setup. (c) Finite element analysis on the rigid steel structure for finding the maximum stresses.

can scan a surface up to a frequency of 200 Hz from 0° to a maximum mirror deflection of 2.86° in a closed feedback control loop operation. The resonance frequency for this mirror is around 1 kHz. An electrodynamic mini-shaker, (B&K Model 4810), is used to generate desired controlled input vibrations. Fixed mirrors at an angle of 45° are used to change the laser optical path in such a way that the laser could scan the human biceps in the horizontal direction. All fixed LDVs and the CSLDV as well as reflective mirrors are mounted on an optical table (Newport Model RS2000-46-8) supported by pneumatic Stabilizer Isolators (Newport Model S-2000 series). The shaker is mounted on a separate table so that shaker excitation could not contaminate the laser data. The settings of all LDVs are set to a scale of maximum velocity of 125 mm/s/V, with low pass filter set at 1 kHz. A National Instruments data acquisition board, (Model cDAQ-9178) is used at a sampling frequency of 10 kHz. Finally, to control all this instrumentation, a LabVIEW software is used. Input and output data signals are recorded at a trigger value set at the maximum value of the

sinusoidal voltage signal applied to the fast scanning mirror.

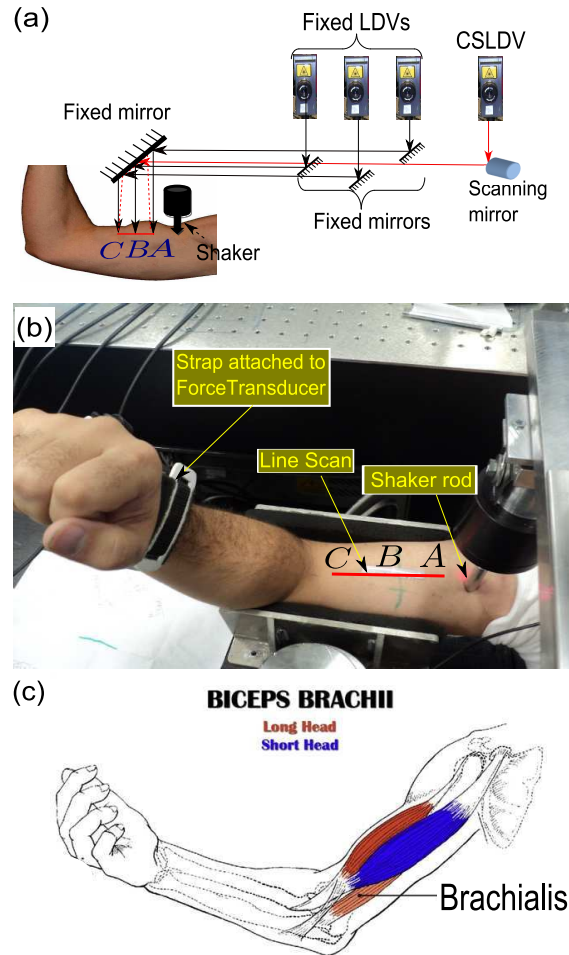


Figure 28: Experimental schematic with complete layout showing 3 fixed LDVs positioned at A,B and C, a CSLDV, a scanning mirror, fixed mirrors, optical path with arrows, a shaker and the biceps. (b) Snapshot of the experimental setup with a 50 mm long line CSLDV on the reflective tape mounted on the biceps brachii and the shaker rod near position A. A strap around the wrist is attached with a force transducer (not shown) fastened with a rigid structure. (c) The physiology of biceps brachii showing the long and short heads and the brachialis. (Reproduced from [28]).

Figure 27b [side view] and Figure 28b [top view] show a snapshot of the biceps contraction setup where a shaker rod is used as an external vibrating source near the proximal end of the long-head of the biceps brachii, and the 50 mm long line CSLDV measures the biceps vibration superficially. The CSLDV scans the retro-reflective tape, (*3MTM*, *ScotchliteTM*, Model 9810) mounted on the biceps. This tape is very thin and flexible and is used to enable the LDV to collect maximum amount of the light scattered back to its photo-detector for

better Doppler signal. Positions A, B and C are used for validating the CSLDV measurements by the three fixed LDVs at A, B and C. There is a strap where the subject can insert his wrist and pull the force transducer, which is attached with a fixed steel structure. The pulling force creates the biceps contractions at different desired levels. Figure 28(c) shows the anatomy of the biceps brachii where the long and short heads are shown in different colors.

4.3 Application to dynamic elastography

4.3.1 Experimental protocol

A simple proof of the concept, an experiment to collect elastography measurements of the biceps brachii of one volunteer subject is presented here, using the CSLDV methodology developed in Chapter 3 [see Figure 28b]. The 24 year old subject was healthy with no overt sign of neuromuscular diseases, and was right handed. This study was conducted according to the protocol approved by the Institutional Review Board of the Georgia Institute of Technology. The right forearm was set at a 90° angle with respect to the upper arm laying flat on a raised support (see Figure 28). A load cell was attached to the subject's wrist to indirectly quantify the force produced by the biceps during isometric contraction by measuring the force generated by the forearm with respect to the elbow joint. First, the MVC force of the subject was measured over a 2 s long contraction while the subject was instructed to produce the maximum contraction. Then, the subject was asked to perform a series of short isometric contractions (2 s long) at 0 %, 20 %, 40 % and 60 % of the MVC levels, while facing a video monitor displaying force output as visual feedback. Subjects were encouraged to rest and relax for 2 min between each contraction in order to minimize artifacts due to muscular fatigue. A total of three trials were performed, where one trial consisted of a randomized order of contraction levels (0 %, 20 %, 40 % and 60 %). Note that 0 % MVC (the reference baseline) corresponds to the absence of contraction of the biceps, i.e., when the muscle is at rest but shaker excites.

The shaker's excitation was manually triggered once the subject reached the required contraction level. The shaker's tip was located on the proximal end of the long-head of the

biceps brachii on the subject’s right arm to generate vibrations propagating along the biceps axis towards the elbow [see Figure 28b]. The shaker’s tip gently pressed the skin’s surface (the indentation depth was set to 5 mm approximately) to slightly compress the superficial skin and fat layer in order to enhance vibration transmission into the underlying biceps muscle. The shaker’s excitation waveform is a one second long LFM in the frequency band [15 Hz to 80 Hz]. The upper excitation frequency is limited by the 100 Hz Nyquist frequency set by the selected scanning frequency $\Omega = 200$ Hz of the tilting mirror for this specific setup. The lowest excitation frequency was limited by the efficiency of the electrodynamic shaker for exciting very low-frequency (< 10 Hz). Finally the CSLDV measured the vibrations emanating from the shaker’s tip and propagating towards the distal end of the subject’s arm (i.e., close to the elbow) along a 5 cm long line scan.

4.3.2 Experimental results

Using the CSLDV methodology explained in Section 3.2.4, the CSLDV signal was demultiplexed to create a line array of virtual sensors distributed along the main axis of the subject’s biceps along a 5 cm long line. Measurements were obtained for a contraction level of 20 % MVC. Overall, Figure 29 shows that the CSLDV can clearly track a propagating pulse (likely associated with transverse propagating waves) along the biceps towards its distal end (i.e., emanating from the shaker location towards the elbow end). Besides, no significant reflected pulse is observed from the end of the biceps muscle, likely due to the high mechanical damping of the musculotendinous junction of the biceps. The peak amplitudes of each pulse are marked on Figure 29 respectively by lozenges and square symbols whether the laser beam moves from extremities A to C or C to A. As expected, the propagation velocity of this pulse appears to be nearly constant since the line scan area overlays a very homogeneous region of the biceps muscle where the muscle fibers run nearly parallel to the arm axis. Thus, the average propagation velocity of the pulse can be readily estimated from the slope of the linear interpolation fitting the peak amplitudes and corresponding arrival times [13]. Finally, for comparison, the matched-filtered waveforms obtained using the three fixed LDVs positioned over locations A, B, C are also indicated, and the peak amplitude

are marked by large circles. Additionally, Figure 29b, c, and d, are the close-up views of the normalized cross-correlations obtained from the three fixed LDVs and the corresponding virtual sensors, whose locations are close to the reference points A, B and C on the biceps. Figure 29 confirms the close agreement between the average propagation velocity estimated either using the line array of virtual sensors $c=5.7$ m/s or the three fixed LDV, $c=6.3$ m/s.

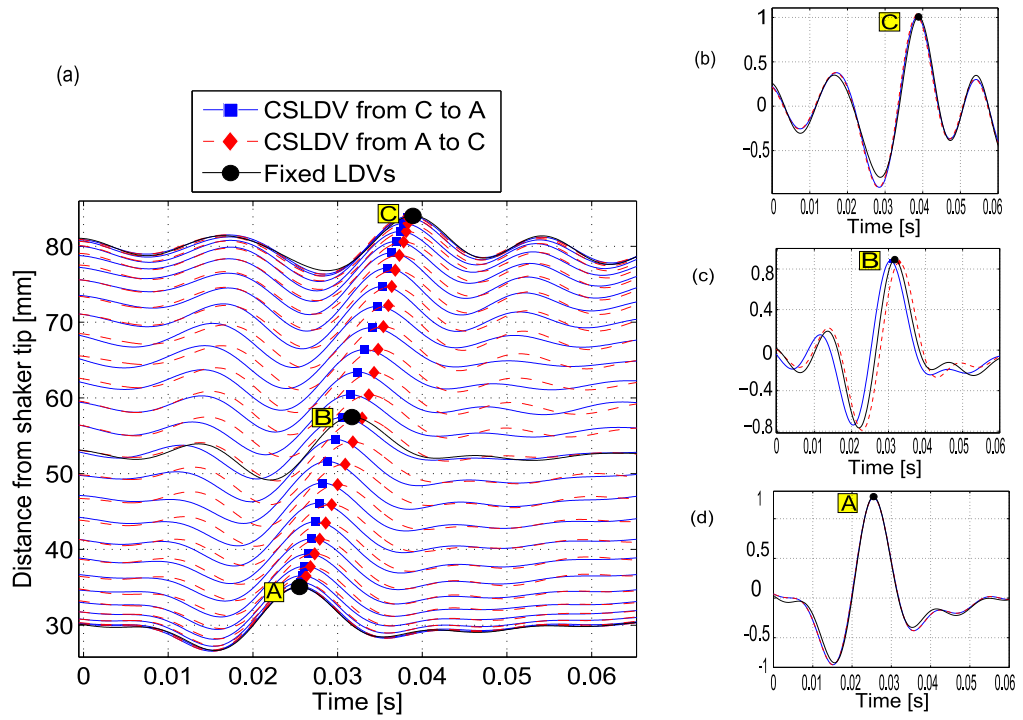


Figure 29: (a) Stacked correlation waveforms for each virtual sensor on the biceps obtained after matched-filtering with a time-shifted and downsampled replica of the shaker LFM excitation. The vertical axis indicates the distance of each of the virtual sensors from the shaker’s tip. (b), (c) and (d) Close-up views of the direct wave arrivals.

4.3.3 Simple biomechanical model

Based on elastography principles, the measured propagation velocity can be used to infer actual elasticity parameters of the soft tissues once a biomechanical model for the pulse propagation is selected [13, 23]. Given the low-frequency content (< 100 Hz) of the excitation vibration and the slow propagation velocity (hence apparent long wavelengths) observed in Figure 29, the simplest propagation model applicable here would be the case of transverse

vibrations propagating over a (viscoelastic) thin rod. But such simple biomechanical models have inherent limitations, as strongly simplifying assumptions must be made regarding the architecture of the tested muscle. However if one is primarily interested in monitoring the relative variations in force level produced by individual skeletal muscles [8], it should be sufficient to monitor the evolution of the average propagation velocity along the tested muscle while the tested muscle is contracting at various levels. In this case, the actual variations of the propagation velocity can then be used as surrogates for inferring the changes in the activity and the contraction level of the tested skeletal muscle [23, 19, 49].

4.3.4 Robustness of the CSLDV technique

The robustness of the proposed CLSDV methodology for monitoring the biceps contraction level and force production is assessed next. To do so, Figure 30 shows the evolution of the arrival times of the propagating pulse along the subject's biceps (and the corresponding propagation velocity) as the contraction level varies from 0 % to 60 % MVC. For each contraction level, horizontal errorbars indicate the standard deviations of the arrival-time measurements at each sensor location (fixed or virtual) across three repeated trials. The linear regression obtained by joining the maximum values of the direct wave arrivals, as shown in Figure 30, gives the surface wave velocity, c_r . The shear wave velocity, c_t , inside the biceps muscle is found from the relationship discussed in Section 3.2.4. The stiffness levels for base line, 20 % MVC, 40 % MVC and 60 % MVC are 39.9 [kPa], 97.4 [kPa], 220.1 [kPa] and 417.6 [kPa] respectively. Overall, the results of Figure 30 support the two main findings: (1) a good repeatability of the propagation velocity measurements derived from the virtual sensors measurements across all three trials, (2) a clear correlation between the measured propagation velocity and the contraction level during isometric contractions of the biceps. Furthermore, these values of the propagation velocities are in quantitative agreement with shear wave velocities measured for the biceps muscle during similar efforts previously obtained using either ultrafast ultrasound elastography [19] or magnetic resonance elastography [16] techniques.

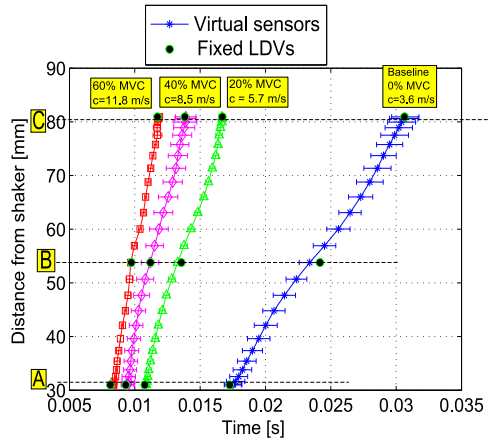


Figure 30: Array of virtual sensors extracted from the CSLDV for the baseline, 20 % MVC, 40 % MVC and 60 % MVC. The horizontal errorbars are obtained from the three sets of data obtained from each contraction level. Fixed LDVs at positions A,B and C are for validation of the CSLDV.

4.3.5 Biceps contraction data for 10 subjects

The trend of the shear wave velocity in the biceps of 10 healthy subjects (male, 24 ± 3 years) was investigated. Each subject's upper arm length was measured from the head of the humerus to the lateral epicondyle. In order to have consistency for each subject, the middle LDV located at point B is always $0.26L$ from the lateral epicondyle where L is the total arm length as shown in Figure 31. The subjects were asked to contract the biceps brachii in an isometric condition (i.e., without changing the muscle length) at different MVC levels. The rest of the protocol for each subject is the same as described in Section 4.3.1.

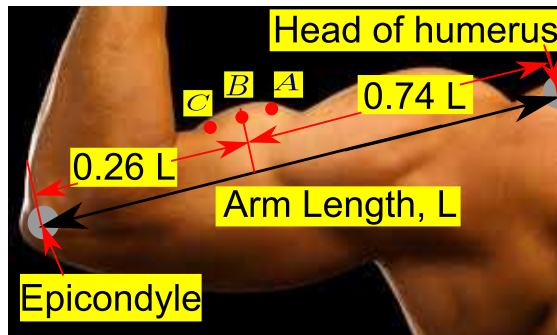


Figure 31: Arm length and marking of three fixed LDVs, A, B and C.

Figure 32a shows the evolution of the actual mean wave velocity of the three trials at

each contraction level. It is obvious that as the biceps contraction level increases, the wave velocity also increases. Figure 32b is plotted for the same data shown in Figure 32a, but it is represented in such a way that the mean wave velocity at each contraction level is divided by the mean velocity of the baseline for each subject (normalized mean phase velocity). The normalized mean phase velocity shows that at 20 % MVC level, the maximum ratio is less than 2.5. Similarly at 40 % MVC and 60 % MVC levels, the maximum ratio is less than 4 and 6 respectively for the 10 subjects.

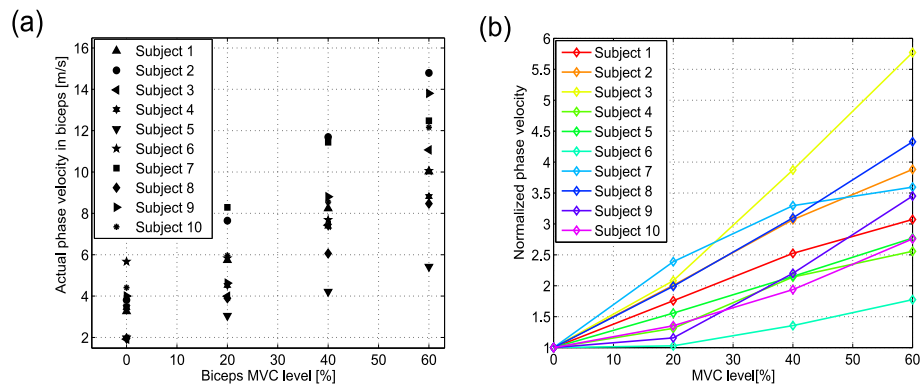


Figure 32: (a) Actual phase velocity in biceps brachii for ten healthy male subjects. (b) Normalized phase velocity in biceps brachii for ten healthy male subjects.

4.3.6 Effect of wrist positions on the biceps stiffness

There is an effect of different wrist positions and elbow joint angles for the biceps isometric contraction on the measured velocities. This effect is studied for 14 healthy male subjects with ages 24 ± 3 years. Figures 33a,c and d show the neutral wrist position (a posture when the wrist and hand are straight) while the elbow joint angle is 90° , 120° and 150° respectively (180° full extension). Figure 33b shows the supination in the forearm which occurs when the palm faces anteriorly (towards the face) while the elbow joint angle is 90° . In this study the protocol is the same as described in Section 4.3.5, but the contraction levels are 0 % MVC, 30 % MVC and 60 % MVC.

The results shown in Figure 34a explain the mean values of the flexural wave velocities on the biceps brachii for four different wrist positions and elbow joint angles. It is clear from the mean velocities that the wrist position with supination 90° has a large mean value

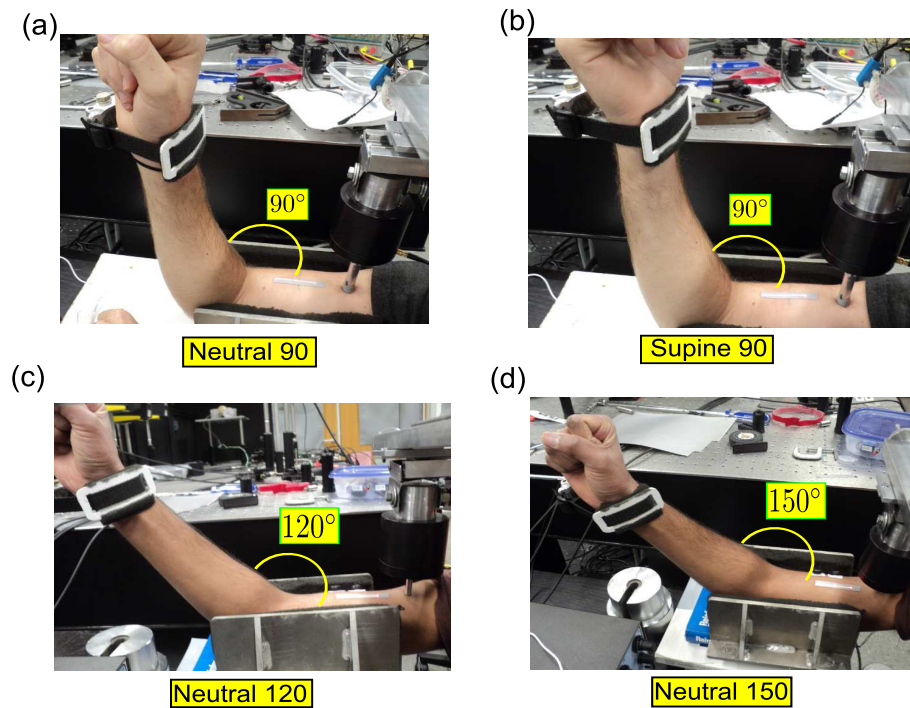


Figure 33: Four different wrist positions and elbow joint angles. (a) Neutral wrist position with elbow joint angle of 90° . (b) Supine wrist position with elbow joint angle of 90° . (c) Neutral wrist position with elbow joint angle of 120° . (d) Neutral wrist position with elbow joint angle of 150° .

as compared to the other three cases. This is true since the biceps brachii in the supine position is in a stiffer state as compared to the other neutral wrist positions. But the fourth wrist position, neutral 150° has a higher mean value of the wave velocity at 60 % MVC level, which is the effect of higher elbow angle and longer muscle. It can be concluded that as the elbow angle increases, which also increases the muscle length, the wave velocity also increases for a given MVC level. Figure 34b shows the errorbars of the velocity ratios. These ratios have been calculated in such a way that the mean velocity of each MVC level for each wrist position is divided by the corresponding mean velocity of neutral wrist position with elbow joint angle of 90° . It is clear from Figure 34b that for the baseline, the ratio supine 90° to neutral 90° is maximum (1.36) as compared to the other ratios. Supine 90° is significantly different from other wrist positions since the biceps is shortened and becomes stiffer in this posture. There is no clear trend of the ratios for the biceps contraction at 30% MVC level, which needs more accuracy in the measurement and consistency of the protocol

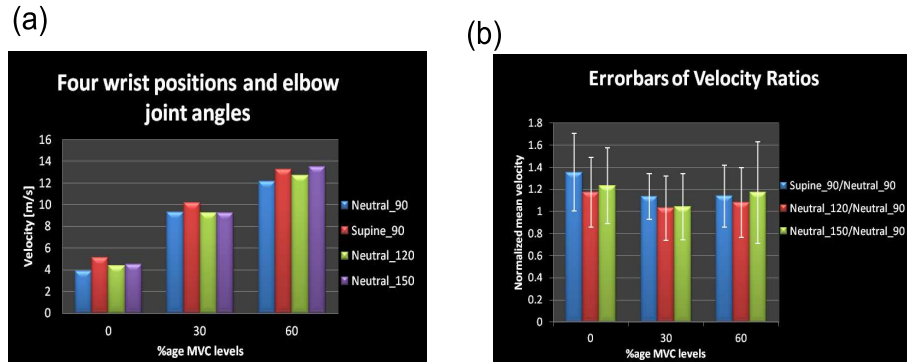


Figure 34: (a) Mean values of the elastic wave velocities for four wrist positions and elbow joint angles obtained at three different biceps MVC levels. (b) Errorbars of the velocity ratios for each wrist position normalized by the corresponding mean values of velocities at neutral wrist position with elbow joint angle of 90° .

for each subject.

4.3.7 Sources of errors and limitations

Tables two to nine show the values for three different MVC levels (0 % MVC, 30 % MVC and 60 % MVC), and each MVC level has three trials for all four positions. The red cells marked in these tables are the values that have $R^2 < 0.9$, while the R^2 value is for the linear regression between the fixed LDVs and the CSLDV measurements. Some of the following parameters limit the accuracy of the CSLDV measurements. Firstly, speckle noise is one of the causes for error in the CSLDV measurements as discussed in Chapter 1. Secondly, the tip of the shaker rod that generates the LFM excitation needs to be positioned along the axis of the biceps with a 5 mm indentation. Tip diameter and the depth of indentation affect the CSLDV measurements. Larger tip diameter at a given depth of indentation produces more excitation energy as compared to the smaller tip. But there is a limitation on the tip diameter, since the assumption of plane wave generation with a large tip diameter is not valid. Thirdly, the muscle fat, which varies a lot from subject to subject. It has been observed that a low fat muscle gives a large value of $R^2 > 0.9$. This is potentially because the muscle fat acts like a damper, which absorbs and attenuates the shaker excitation. Fourthly, the upper arm should be as horizontal as possible and should be perpendicular to the LDVs. Human error is involved in producing precise and accurate alignments for the

exact perpendicularity of the LDVs as well as the exact elbow joint angles for each subject. Finally, muscle fatigue is another limitation on the CSLDV measurements, this is why after each contraction data collection, there is a certain relaxation time given to the subject.

Table 2: Data for neutral 90° elbow joint angle

MVC	0%	0%	0%	30%	30%	30%	60%	60%	60%
Subject 1	4.02	3.07	3.02	10.27	12.88	13.66	11.21	15.03	15.31
Subject 2	2.28	2.40	1.55	5.48	5.82	6.41	9.57	10.82	13.65
Subject 3	4.22	4.01	3.96	5.82	6.50	7.49	11.77	8.26	6.43
Subject 4	5.52	7.23	4.29	14.20	12.90	13.36	13.44	17.90	13.27
Subject 5	2.49	2.53	2.33	5.90	5.62	6.09	7.17	8.64	7.32
Subject 6	7.69	x	4.00	9.41	9.13	11.09	13.63	12.93	12.64
Subject 7	x	3.49	3.60	12.67	10.84	11.66	19.89	16.08	17.60
Subject 8	3.67	3.48	3.34	4.83	5.88	6.98	7.49	8.31	8.12
Subject 9	3.38	2.80	2.95	6.75	9.27	8.22	11.41	11.92	10.44
Subject 10	4.07	4.59	5.39	7.77	8.80	8.57	14.14	11.85	9.35
Subject 11	4.15	4.35	3.96	6.46	6.61	8.18	8.57	8.36	8.43
Subject 12	4.59	4.95	4.94	8.59	20.35	16.61	20.12	x	17.73
Subject 13	4.70	4.36	4.18	6.65	5.97	7.83	8.71	8.97	8.57
Subject 14	2.29	2.52	2.46	10.34	14.25	14.60	15.21	16.28	15.63

Table 3: R-Squared value for neutral 90° elbow joint angle

MVC	0%	0%	0%	30%	30%	30%	60%	60%	60%
Subject 1	0.996	0.999	0.999	0.987	0.992	0.991	0.991	0.990	0.992
Subject 2	0.998	0.995	0.643	0.999	0.997	0.981	0.997	0.995	0.998
Subject 3	0.972	0.993	0.992	0.974	0.987	0.978	0.988	0.985	0.991
Subject 4	0.995	0.996	0.999	0.937	0.943	0.982	0.870	0.981	0.958
Subject 5	0.985	0.987	0.997	0.993	0.994	0.982	0.995	0.985	0.966
Subject 6	0.954	0.697	0.952	0.991	0.985	0.979	0.981	0.946	0.975
Subject 7	0.808	1.000	1.000	0.995	0.997	0.993	0.989	0.995	0.979
Subject 8	0.999	0.999	0.999	0.998	0.992	0.998	0.994	0.991	0.995
Subject 9	0.998	0.998	0.994	0.997	0.993	0.997	0.984	0.992	0.996
Subject 10	0.998	0.998	0.995	0.989	0.993	0.994	0.981	0.978	0.978
Subject 11	0.999	0.998	0.942	0.980	0.980	0.992	0.982	0.992	0.984
Subject 12	0.998	0.993	0.997	0.976	0.916	0.990	0.975	0.881	0.931
Subject 13	0.997	0.997	0.999	0.999	0.998	0.997	0.997	0.998	0.999
Subject 14	0.999	0.995	0.991	0.987	0.982	0.981	0.993	0.970	0.931

Table 4: Data for supine 90° elbow joint angle

MVC	0%	0%	0%	30%	30%	30%	60%	60%	60%
Subject 1	3.41	3.82	4.01	13.25	15.40	13.24	12.68	13.99	11.88
Subject 2	3.04	4.70	3.99	6.30	8.94	7.75	15.07	14.86	15.56
Subject 3	5.14	4.75	5.88	7.80	7.91	9.40	10.88	11.90	13.07
Subject 4	4.11	8.38	6.32	13.74	16.26	12.62	10.11	x	x
Subject 5	4.87	5.91	4.32	7.92	10.53	9.87	10.04	12.56	10.62
Subject 6	x	6.99	8.10	11.93	x	10.64	13.79	x	13.12
Subject 7	6.89	4.33	4.20	13.42	13.76	14.15	15.82	21.76	19.71
Subject 8	4.66	4.42	4.12	5.55	7.30	6.75	8.41	10.19	9.45
Subject 9	3.58	4.24	3.99	7.34	12.43	11.74	22.12	13.53	15.04
Subject 10	6.01	6.94	5.59	6.96	7.51	8.66	9.26	9.82	9.03
Subject 11	4.90	3.36	4.10	9.75	7.10	7.48	14.80	14.24	13.87
Subject 12	7.22	11.37	9.16	10.40	12.68	10.45	20.52	18.56	14.97
Subject 13	4.45	4.75	4.42	6.79	6.86	6.64	9.44	8.29	8.19
Subject 14	2.01	2.80	x	10.88	13.17	14.86	17.79	15.05	9.90

Table 5: R-Squared value for supine 90° elbow joint angle

MVC	0%	0%	0%	30%	30%	30%	60%	60%	60%
Subject 1	1.000	1.000	1.000	0.986	0.990	0.990	0.980	0.998	0.996
Subject 2	0.995	0.999	0.993	0.999	1.000	0.997	0.998	0.998	0.995
Subject 3	0.995	0.975	0.983	0.994	0.975	0.980	0.996	0.988	0.973
Subject 4	0.956	0.942	0.984	0.978	0.992	0.991	0.985	0.283	-0.089
Subject 5	0.983	0.948	0.981	0.996	0.998	0.999	0.995	0.978	0.994
Subject 6	-0.104	0.911	0.970	0.940	0.836	0.898	0.970	0.010	0.975
Subject 7	0.996	0.999	0.999	0.997	0.993	0.996	0.995	0.975	0.984
Subject 8	0.996	0.996	0.995	0.997	0.999	1.000	0.995	0.998	0.999
Subject 9	1.000	0.999	0.998	0.985	0.982	0.992	0.982	0.988	0.944
Subject 10	0.998	0.998	0.997	0.999	0.993	0.992	0.997	0.997	0.997
Subject 11	0.997	0.992	0.999	0.971	0.982	0.981	0.958	0.876	0.872
Subject 12	0.987	0.983	0.979	0.992	0.984	0.968	0.886	0.955	0.995
Subject 13	0.995	0.998	0.998	0.996	0.994	0.998	0.998	0.996	0.996
Subject 14	0.962	0.964	0.890	0.985	0.982	0.969	0.927	0.931	0.971

Table 6: Data for neutral 120° elbow joint angle

MVC	0%	0%	0%	30%	30%	30%	60%	60%	60%
Subject 1	3.70	4.19	3.69	9.25	8.05	8.14	12.22	10.57	12.34
Subject 2	2.35	2.40	2.87	7.79	8.86	9.07	14.76	13.10	11.52
Subject 3	3.95	4.20	4.15	5.11	6.26	4.95	7.32	8.51	9.51
Subject 4	10.31	7.35	8.26	19.67	22.23	17.75	25.11	19.35	22.97
Subject 5	3.33	2.96	2.93	6.48	6.54	6.35	7.89	10.23	9.46
Subject 6	6.29	4.80	5.33	8.28	6.94	8.19	9.92	9.93	9.44
Subject 7	3.92	4.70	4.95	12.27	11.76	14.54	21.63	16.97	21.56
Subject 8	4.59	5.01	4.61	8.54	8.64	8.85	12.97	14.16	17.06
Subject 9	5.79	5.58	5.84	8.13	9.19	8.00	9.05	9.45	10.90
Subject 10	3.47	3.32	3.00	7.62	9.26	7.75	11.41	16.11	11.99
Subject 11	3.53	3.57	3.52	6.89	6.41	5.13	9.66	9.88	7.05
Subject 12	4.23	2.01	4.93	8.07	7.71	7.91	12.22	10.52	10.55
Subject 13	5.12	5.03	5.12	7.53	6.65	9.13	10.40	10.61	9.45
Subject 14	3.54	3.19	3.10	12.84	12.74	13.07	13.59	15.27	16.96

Table 7: R-Squared value for neutral 120° elbow joint angle

MVC	0%	0%	0%	30%	30%	30%	60%	60%	60%
Subject 1	0.999	0.998	0.999	0.999	0.999	0.998	0.995	0.991	0.991
Subject 2	0.996	0.993	0.998	0.999	0.999	0.998	0.992	0.995	0.996
Subject 3	1.000	0.998	0.999	0.997	0.998	0.999	0.987	0.996	0.997
Subject 4	0.992	0.993	0.997	0.994	0.980	0.989	0.993	0.995	0.963
Subject 5	0.992	0.991	0.995	0.999	0.999	0.995	0.997	0.993	0.994
Subject 6	0.998	0.997	0.998	0.997	0.999	0.999	0.975	0.970	0.981
Subject 7	1.000	1.000	0.999	0.999	0.999	0.995	0.997	0.995	0.994
Subject 8	0.998	0.996	0.999	0.997	0.997	0.998	0.997	0.982	0.997
Subject 9	1.000	0.998	0.998	0.997	0.991	0.999	0.997	0.993	0.915
Subject 10	0.999	0.999	1.000	0.995	0.992	0.999	0.989	0.970	0.994
Subject 11	0.999	0.999	0.998	0.998	1.000	0.999	0.999	0.998	0.983
Subject 12	0.998	0.998	0.993	0.997	0.994	0.994	0.997	0.999	0.991
Subject 13	1.000	0.999	0.999	0.999	0.997	0.997	0.997	0.996	0.982
Subject 14	0.996	0.999	0.995	0.974	0.994	0.992	0.988	0.995	0.975

4.4 Summary and conclusions

This chapter uses the CSLDV technique to demonstrate the applicability of the proposed CLSDV methodology for measuring the velocity of a low-frequency flexural wave propagating along the biceps brachii muscle of 10 to 14 volunteer subjects. The effect of four wrist positions and elbow joint angles were studied over the stiffness change of the biceps. The increase in propagation velocity was found to be closely correlated with the increase in force produced by the subject while performing short isometric contractions of increasing

Table 8: Data for neutral 150° elbow joint angle

MVC	0%	0%	0%	30%	30%	30%	60%	60%	60%
Subject 1	4.98	4.88	5.20	7.98	8.21	9.17	11.10	11.47	9.23
Subject 2	3.92	3.09	3.79	8.29	7.93	9.12	12.66	12.12	13.46
Subject 3	4.65	3.12	3.58	5.06	5.35	4.53	5.28	5.18	6.65
Subject 4	10.25	6.39	8.48	16.42	15.34	20.00	19.81	25.67	22.04
Subject 5	3.82	3.37	3.27	7.31	7.64	8.53	11.54	17.16	16.33
Subject 6	5.01	5.95	4.80	10.73	9.52	8.69	9.07	11.05	9.78
Subject 7	x	x	4.55	9.70	8.65	9.34	15.38	12.03	15.26
Subject 8	5.78	6.24	5.92	7.90	7.42	7.14	9.69	12.43	10.28
Subject 9	4.11	3.78	3.92	11.05	11.19	10.65	x	12.76	21.44
Subject 10	4.35	4.61	4.06	10.83	11.74	12.74	21.15	20.57	25.64
Subject 11	3.22	4.48	4.68	7.66	6.33	5.92	12.98	19.65	8.34
Subject 12	4.56	4.45	4.36	8.02	7.94	8.48	10.14	10.09	9.85
Subject 13	3.10	2.74	2.87	5.46	6.15	6.22	7.87	10.73	7.85
Subject 14	4.02	3.57	3.64	11.53	12.60	13.54	15.55	15.77	17.56

Table 9: R-Squared value for neutral 150° elbow joint angle

MVC	0%	0%	0%	30%	30%	30%	60%	60%	60%
Subject 1	0.998	0.999	0.999	0.996	0.985	0.989	0.991	0.996	0.999
Subject 2	0.998	0.998	0.995	0.998	0.998	0.998	0.993	0.992	0.999
Subject 3	0.963	0.984	0.991	0.997	0.992	0.970	0.954	0.991	0.970
Subject 4	0.990	0.999	0.999	0.989	0.994	0.985	0.987	0.995	0.996
Subject 5	0.998	0.992	0.998	0.995	0.996	0.997	0.994	0.983	0.994
Subject 6	1.000	1.000	0.998	0.989	0.998	0.993	0.989	0.986	0.997
Subject 7	0.213	0.893	0.996	0.999	1.000	0.999	0.997	0.999	0.999
Subject 8	1.000	0.999	0.999	0.997	0.999	0.999	0.986	0.998	0.999
Subject 9	1.000	0.999	1.000	0.998	0.997	0.998	0.796	0.986	0.962
Subject 10	0.994	0.997	0.998	0.990	0.995	0.986	0.985	0.992	0.970
Subject 11	0.995	0.997	0.999	0.993	0.999	0.984	0.988	0.900	0.996
Subject 12	0.999	0.999	1.000	0.995	0.998	0.984	0.994	0.994	0.998
Subject 13	1.000	1.000	1.000	0.999	0.999	0.996	0.996	0.994	0.998
Subject 14	0.998	0.996	0.996	0.993	0.984	0.983	0.987	0.991	0.998

intensity. Hence, this CSLDV methodology could provide a low-cost elastography modality for clinical practice to assess the stiffness of individual skeletal muscles, and thus ultimately their individual force production during various tasks.

CHAPTER V

CONCLUSIONS AND FUTURE WORK

5.1 Summary

This research has developed a Continuous Scanning Laser Doppler Vibrometer (CSLDV) technique, based on a single laser beam continuously sweeping the area of interest using a scanning mirror. Two major types of scans were validated, one- short scan (line and circular waveforms) and the second one- long scan (line waveform). Short scans were used for measuring the multiple DOF of low broadband frequency vibrations of hand tremors during a sustained and fatiguing task. The parameters effecting the “speckle noise” were investigated and addressed in order to improve the accuracy of the CSLDV technique. The second part of this research develops the long line CSLDV technique (≥ 5 cm). This long line CSLDV was used for the replacement of an array of vibration sensors by a single long line scan CSLDV. It was applied to measure the forced vibrations on the biceps brachii in order to find the muscle stiffness. The effects of different wrist positions and elbow joint angles were investigated for the biceps stiffness levels at various MVC levels.

5.2 Key Contributions

Three main contributions were achieved from this research.

1. A short scan CSLDV technique was developed to find the low frequency broadband measurement (≤ 100 Hz) of the human skeletal muscles. This is new knowledge and a variant approach of demodulating the translational and rotational DOF of hand tremors during a sustained task against the gravity. These contributions have been disseminated to the community as the following publication: “Broadband measurement of translational and angular vibrations using a single continuously scanning laser Doppler vibrometer”. Muhammad Salman and Karim G. Sabra. *Journal of Acoustical Society of America*, (2012).

2. A long scan CSLDV technique applied a demultiplexing algorithm to extract an array of virtual velocity sensors over the scanned surface. This technique is especially advantageous for sensing natural vibrations of the human body at multiple locations (e.g., along small muscles), as it does not require traditional skin-mounted sensors (e.g., accelerometers array). It thus eliminates mass artifacts and the setup time to attach those sensors. These contributions have been submitted and are under review by the *Journal of Acoustical Society of America*, “Synchronized surface vibrations measurements using a single continuously scanning Laser Doppler Vibrometer: Application to elastography of skeletal muscles”. Muhammad Salman and Karim G. Sabra.
3. This CSLDV technique is applied to measure the elastic stiffness of the human skeletal muscle such as biceps brachii. Muscle stiffness is measured on the basis of the apparent velocity of low-frequency flexural waves excited by a shaker propagating along the biceps brachii axis. Data for biceps dynamic elastography has been collected and investigated from 10 to 14 male subjects for different contraction levels at four different wrist positions and elbow joint angles. Ultimately, this CSLDV technique could then be used to provide a simple, affordable, noninvasive and in vivo elastography modality for quantitative measurements of muscles’ tone (or stiffness) and thus potentially improve the objective diagnosis of musculoskeletal and neuromuscular disorders in clinical practice.

5.3 Recommendations for Future Research

Following are the recommendations provided for future work about the measurement of elastic stiffness using this long scan CSLDV technique.

1. This study uses the CSLDV technique for the dynamic elastography, which is the measurement of shear wave velocity by using an external source of vibration. It is recommended to use this technique for passive elastography where there is no use of external vibrating source.
2. There were some limitations in this study, such as the scanning frequency of the

mirror, which was limited to 200 Hz, and the scanning length, which was less than 6 cm. It is recommended to use a faster scanning frequency of a mirror with a large covering area in order to have more high frequency broad band measurements.

3. This research used mostly a line scan CSLDV, while there are other types of scanning waveforms which give more scanning area and more control over the measurements of varying bandwidth frequency vibrations such as Lissajous scan, spiral scan, elliptical scan etc. Each scan type needs a different data processing algorithm for demodulating a specific DOF of vibration. It is recommended to use these different types of scanning waveforms for the measurement of multiple DOF of vibrations.
4. This study aimed at implementing the CSLDV technique for estimating the stiffness of human skeletal muscle such as biceps. This elastography technique relies on measuring the propagation velocity of mechanical vibrations (primarily flexural waves here) along skeletal muscles (biceps brachii here). However one would need to develop an accurate biomechanical and rheological model of the biceps muscle in order to infer the actual muscle stiffness from the velocity measurement.
5. There were some limitations in the biceps contraction fixture, such as the shaker rod tip, exact alignment of the CSLDV and the fixed LDVs and the speckle noise. It is recommended to use more varied design of the shaker rod tip, which could generate high energy flexural waves for the best CSLDV measurements. More time and effort are required to check different sampling frequencies at a given scanning frequency in order to see their effects on the spatial resolution for the virtual array of sensors extracted from the long line CSLDV.
6. This long line CSLDV technique used the method of sensing 50 virtual locations in a 5 cm scan length. It used a linear fit for all those 25 sensors back and forth. It is recommended to break these sensors into different segments (e.g., first eight sensors followed by 10 sensors and then finally seven sensors) in order to see the velocity of the propagating flexural wave separately in each segment, this could give more piecewise information.

7. It is recommended to use this CSLDV technique in combination with the ElectroMyoGram (EMG) signals, which are signals for evaluating the electrical activity generated from the central nervous system for skeletal muscles to see musculoskeletal disorder. The relationship between the mechanical oscillations also known as surface MechanoMyoGrams (sMMG) and the EMG signals needs to be explored further.
8. This research has applied this CSLDV technique over the human biceps brachii. It is recommended to use this technique over the musculotendinous area or over tendons such as Achilles tendon in order to have more results concerning the stiffness of these bio-materials.
9. This study investigated the stiffness of biceps brachii from healthy male subjects only. It is recommended to explore the same type of data from female subjects.
10. There is a connection between the stiffness of human skeletal muscles and the rehabilitation and training exercise for handicapped people. It is recommended to further explore this connection which could give clinicians more deep understanding about the skeletal muscle stiffness behavior.
11. Muscles get fatigued after a certain contraction period. The stiffness changes of skeletal muscles during the fatigue state needs to be further explored. More time and efforts are required to collect data for the stiffness changes before, during and after a fatigue task.

APPENDIX A

LDV PRINCIPLE

A.1 Laser light and the Doppler shift

A laser has coherent optical signal emitted at a precise frequency f_o , where $f_o = c_o/\lambda_o$ and c_o is the speed of light in a vacuum. Usually an LDV has its source from Helium Neon Laser (He-Ne). The wavelength, λ_o , for He-Ne laser is = 632.8 nm and $f_o = 4.74 * 10^{14}$ Hz (red light). Coherence refers to the spatial characteristics of the light wave. Coherence time, T_c , for example, is the time interval during which the plane of the signal does not change. Corresponding to this time period, T_c , the laser coherence length, $L_c = c_o T_c$. Although the frequency of the laser is very precise, its frequency spectrum is not a single line. It has spectral line width, Δf which is ≈ 1 GHz.

A.1.1 Doppler effect

When a propagating wave (acoustic, optical) is reflected by a moving object as shown in Figure A.1, the wave equation is described by the Eq. (18).

$$S = S_o \cos(\omega_o t - k_o x) = S_o \cos(\phi(t, x)) \quad (18)$$

Where ω_o is the temporal frequency and k_o is the spatial frequency. The instantaneous angular frequency is $\omega = d\phi/dt$. If the surface velocity is zero, the reflected signal at the LDV is given as in Eq. (19) where $\omega = \omega_o$.

$$S = S_o \cos(\omega_o t - 2k_o L) \quad (19)$$

When the surface is moving, i.e., $V \neq 0$: the traveling wave, S is described by the Eq. (20), where L is the distance from the laser head to the test object and ΔL is the reduction in path length due to the motion of the object.

$$S = S_o \cos(\omega_o t - 2k_o(L - \Delta L)) \quad (20)$$

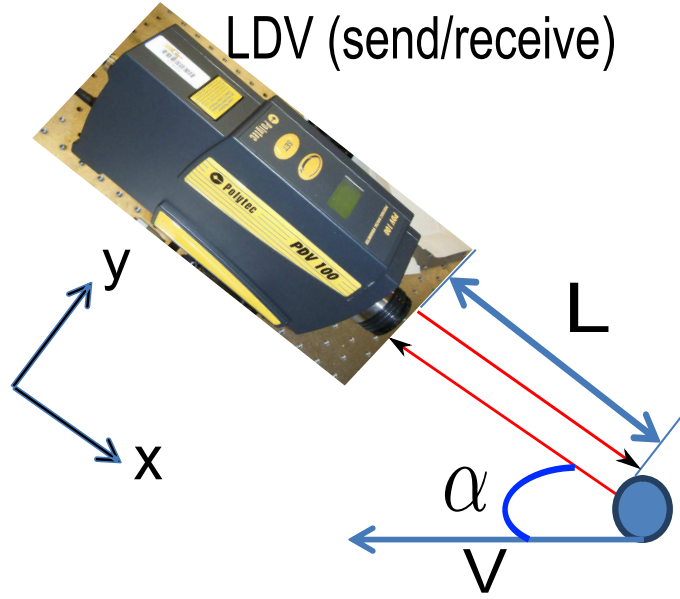


Figure A.1: Doppler effect when the laser beam scatters back from a moving surface.

Now in this case ω is given in Eq. (21)

$$\omega = \omega_o 2k_o \frac{\partial(\Delta L)}{\partial t} = \omega_o + 2k_o v \cos \alpha \quad (21)$$

Eq. (22) shows the Doppler frequency, ω_D and if the displacement is in x-axis then $\omega_D = \frac{4\pi}{\lambda} v$.

$$\omega_D = 2k_o v \cos \alpha = \frac{4\pi}{\lambda} v \cos \alpha \quad (22)$$

Consider a laser beam normally incident on a moving surface, the Doppler shift as given in the Eq. (22), describes that the Doppler frequency, $f_D > \Delta f$. After simplifying and substituting the values in this inequality, $f_D > \Delta f$, the Doppler velocity is in the order of 316 m/s which is too large for most applications. (Typically acoustics velocity is on the order of mm/s). The solution to this problem is the use of Michelson Interferometer.

A.1.2 Interferometry

Michelson Interferometer detects out-of-plane (i.e., Normal to the surface) vibration. Basic idea is to split the beam into two paths, one reference path and the other one returning path, and then to recombine the two beams to create an interference signal. A homodyne

interferometry uses a single-frequency laser source, which is He-Ne in case of an LDV (see Figure A.2(a)). A heterodyne interferometry uses a laser source with two close frequencies. The heterodyne interferometry has an advantage over homodyne interferometry such as removing noise at low frequencies coming from other sources such as power supplies etc. A Bragg cell is used for a frequency shift, ω_B as shown in Figure A.2(b), which acts like a carrier frequency, and a constant modulation intensity of a resting surface at the photo detector. If a vibrating surface is moving towards the laser, the modulation frequency is greater than 40 MHz and if the target surface is moving away from the laser then modulation frequency is smaller than 40 MHz. This phenomena is expressed in Eq. (29) where $f_{detector}$ is the frequency at the photodetector, 40 MHz is the career frequency of the Bragg cell and f_D is the Doppler frequency shift due to the target movement. Bragg cell frequency acts as a zero crossing which means the non-linear behavior of a photodiode due to intensity effects does not change the Doppler signal.

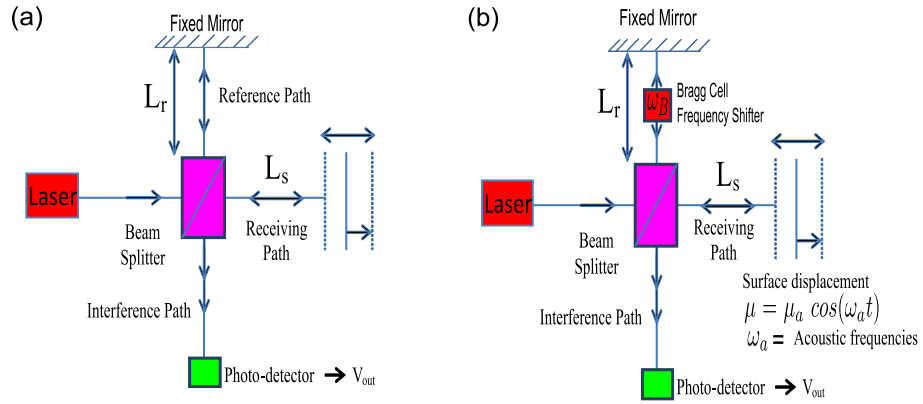


Figure A.2: Michelson interferometry principle. (a) Homodyne interferometry. (b) An LDV uses heterodyne interferometry principle with He-Ne laser (wavelength of 632.8 nm).

The optical signals are described by their electric field as given by

$$E_r = E_{or} \cos(\omega_o t - 2k_o L_r) \quad (23)$$

$$E_s = E_{os} \cos(\omega_o t - 2k_o L_s - 2k_o \mu) \quad (24)$$

L_r in Eq. (23) is the reference path length and L_s in Eq. (24) is the receiving path

length. The displacement of a moving surface is represented by μ in Eq. (24). In order for these two signals to interface coherently, the path length difference ($L_s - L_r$) must be less than the coherence length L_c of the laser. $L_c = 30$ cm for He-Ne laser.

Assuming that $(L_s - L_r) < L_c$, the two beams interface at the face of the beam splitter and the receiving signal is measured by the photo-detector, which produces a voltage V_{out} proportional to the light intensity (i.e., square of the electric field). The photo-detector takes a time average of the intensity. V_{out} is given in Eq. (25), (26), where A is the photo-detector constant.

$$V_{out} = A \langle (E_r + E_s)^2 \rangle \quad (25)$$

$$V_{out} = A \langle (E_r^2 + E_s^2 + 2E_r E_s) \rangle \quad (26)$$

$$V_{out} = A[1/2(E_{or}^2 + E_{os}^2) + 2E_{or}E_{os}\cos(2k_o(L_s - L_r) + 2k_o\mu)] \quad (27)$$

$$V_{out} = C\cos(2k_o(L_s - L_r) + 2k_o\mu)] \quad (28)$$

After filtering out the DC term from Eq. 27, the output voltage is given by Eq. (28). Introducing the phase term in Eq. (28) as $\phi = 2k_o(L_s - L_r)$, that randomly fluctuates because of ambient mechanical and thermal fluctuations (Low frequency fluctuations). The photo-detection output is proportional to the acoustic displacement μ , but its amplitude is multiplied by $\sin \phi$, fades in and out randomly. In order to avoid this problem, heterodyne interferometry is introduced in the LDV.

A.1.3 Heterodyne Interferometry

A heterodyne interferometry uses a laser source with two close frequencies. The heterodyne interferometry has an advantage over homodyne interferometry such as removing noise at low frequencies coming from other sources such as power supplies etc. A Bragg cell is used for a frequency shift, ω_B as shown in Figure A.2b, which acts like a carrier frequency, and a constant modulation intensity of a resting surface at the photo detector. If a vibrating

surface is moving towards the laser, the modulation frequency is greater than 40 Mhz and if the target surface is moving away from the laser then modulation frequency is smaller than 40 MHz. This phenomena is expressed in Eq. (29) where $f_{detector}$ is the frequency at the photodetector, 40 MHz is the carrier frequency of the Bragg cell and f_D is the Doppler frequency shift due to the target movement. Bragg cell frequency acts as a zero crossing which means the non-linear behavior of a photodiode due to intensity effects does not change the Doppler signal.

$$f_{detector} = (40MHz \pm f_D) \quad (29)$$

$$E_r = E_{or} \cos((\omega_o + \omega_B)t - 2k_o L_r) \quad (30a)$$

$$V_{out} = C \cos(\omega_B t + 2k_o \mu + \phi) \quad (30b)$$

The new energy signal for the reference beam at the photo-detector due to the back scattered light is given by Eq. (30a). C is the photo-detector sensitivity constant related to its efficiency. The voltage output is now a signal at the frequency ω_B (called the carrier frequency) as shown in Eq. (30b), modulated by the Doppler shift $2k_o \mu$, with a low frequency varying phase term, ϕ . A high-pass filter can be used to eliminate ϕ and get a stable signal at ω_B .

A.1.4 Demodulation of Doppler signal

In order demodulate a Doppler shifted signal of the LDV, a phase-locked loop circuit (PLL) can be used as shown in Figure A.3. A PLL basically locks on the frequency of the input signal and produces an output voltage proportional to the rate of change of the phase, $d\phi/dt$ of the input. The phase difference detector as shown in the Figure A.3 compares f_{in} and f_{vco} and after time Δt , it produces a voltage proportional to $f_{in} - f_{vco}$. This voltage is then low pass filtered, amplified and fed into the voltage controller oscillator (VCO) (see Figure A.3), which adjusts f_{vco} according to its input voltage. After a few Δt , the VCO adjusts its frequency according to f_{in} . Then the output voltage of the PLL is a signal proportional to $f_{in} - f_{vco}$ as shown in Eq. (31a).

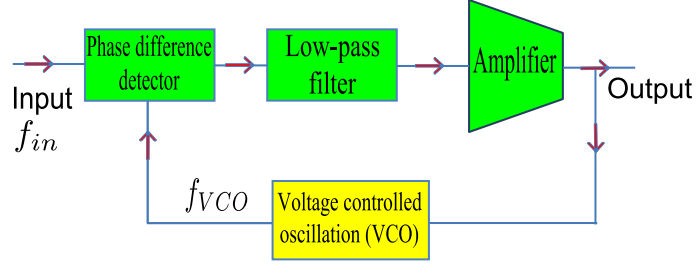


Figure A.3: Phase-Locked Loop (PLL) circuit used for demodulating the Doppler shift measured by the laser beam of the LDV.

$$V_{out,PLL} = f_{in} - f_{vco} = \frac{1}{2\pi} \left(\frac{d\phi_{in}}{dt} - \frac{d\phi_{out}}{dt} \right) \quad (31a)$$

$$V_{out,PLL} = C \frac{d}{dt} (\omega_B t + 2k_o \mu - \omega_B t) \quad (31b)$$

$$V_{out,PLL} = K 2k_o v \quad (31c)$$

The PLL output voltage given in Eq. (31c) is obtained after simplifying Eq. (31b) and is proportional to the instantaneous surface velocity where K is the photo-detector constant.

APPENDIX B

SHORT SCAN

B.1 Data Acquisition Setup

A National Instruments data acquisition board, (cDAQ-9178 with 8 input/output module slots) as shown in the Figure B.4a was used to simultaneously sample all LDVs signals with a sampling rate of 10 kHz using the labVIEW software as shown in Figure B.4b.

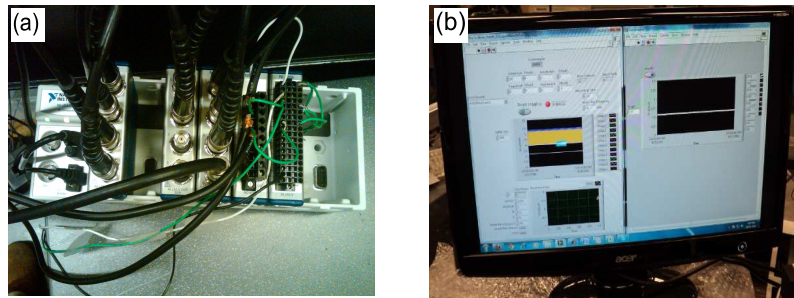


Figure B.4: (a) A National Instruments data acquisition board, (cDAQ-9178 with 8 input/output module slots). (b) LabVIEW user interface for integrating the equipment.

B.2 Comparison of speckle noise for fixed LDV and the CSLDV

Figure B.5a illustrates the comparison of the speckle noise levels for the baselines of the CSLDV and the fixed LDV on a logarithmic scale. Here the scan length is 1 cm and the shaker excites an LFM signal in the frequency band of [10 Hz to 50 Hz]. Signal strength is stronger as compared to the both baselines. Figure B.5b is similar to Figure B.5a but only compares the baselines for both the CSLDV and the fixed LDV output in the frequency band of B_n (see Figure 8) on a linear scale.

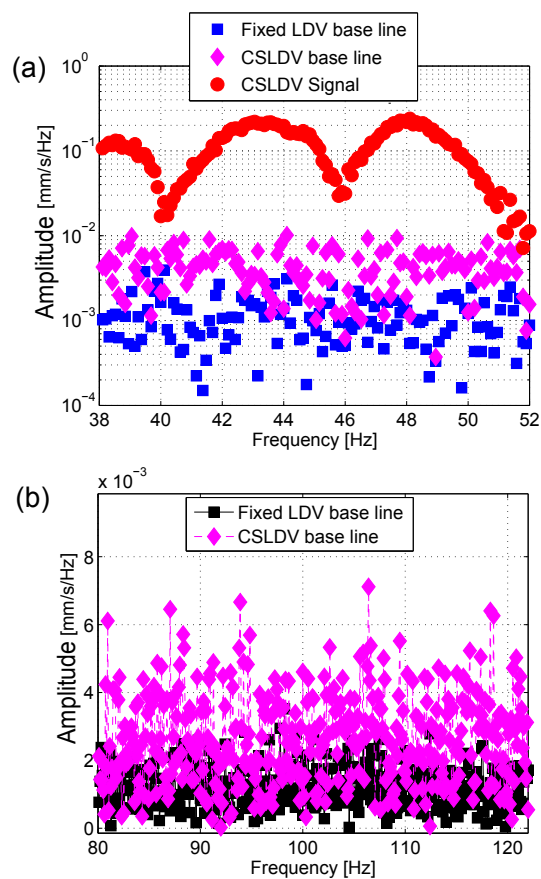


Figure B.5: (a) Comparison of baselines for the CSLDV and the fixed LDV with the CSLDV signal on the logarithmic scale (b) Comparison of baselines for the CSLDV and the fixed LDV in the frequency band, B_n [80 Hz to 120 Hz].

REFERENCES

- [1] ALLEN, M. S. and SRACIC, M. W., “A new method for processing impact excited continuous-scan laser Doppler vibrometer measurements,” *Mechanical Systems and Signal Processing*, vol. 24, no. 3, pp. 721–735, 2010.
- [2] ALLEN, M. S., SRACIC, M. W., CHAUHANB, S., and HANSEN, M. H., “Output-only modal analysis of linear time periodic systems with application to wind turbine simulation data,” *Mechanical Systems and Signal Processing*, vol. 25, pp. 1174–1191, 2011.
- [3] ARANCHUK, V., LAL, A., HESS, C., and SABATIER, J. M., “Multi-beam laser doppler vibrometer for landmine detection,” *Optical Engineering*, vol. 45, no. 10, 2006.
- [4] ARCHER, A. A., ATANGCHO, P., SABRA, K. G., and SHINOHARA, M., “Propagation direction of natural mechanical oscillations in the biceps brachii muscle during voluntary contraction,” *Journal of Electromyography and Kinesiology*, vol. 22, pp. 51–59, 2011.
- [5] BASFORD, J., JENKYN, T., AN, K., EHMAN, R. L., HEERS, G., and KAUFMAN, K. R., “Evaluation of healthy and diseased muscle with magnetic resonance elastography,” *Archives of Physical Medicine and Rehabilitation*, vol. 83(11), pp. 1530–1536, 2002.
- [6] BELL, J. and ROTHBERG, S., “Rotational vibration measurements using laser Doppler vibrometry: Comprehensive theory and practical application,” *Journal of Sound and Vibration*, vol. 238, pp. 673–690, DEC 7 2000.
- [7] BENSAMOUN, S., GLASER, K., RINGLEB, S., CHEN, Q., EHMAN, R., and AN, K., “Rapid magnet resonance elastography of muscle using one-dimensional projection,” *Journal of Magnetic Resonance Imaging*, vol. 27, pp. 1083–1088, 5 2008.
- [8] BOUILLARD, K., NORDEZ, A., and HUG, F., “Estimation of individual muscle force using elastography,” *PLoS ONE*, vol. 6(12), no. 12, p. e29261, 2011.
- [9] CASTELLINI, P., MARTARELLI, M., and TOMASINI, E., “Laser Doppler Vibrometry: Development of advanced solutions answering to technology’s needs,” *Mechanical System and Signal Processing*, vol. 20, pp. 1265–1285, AUG 2006.
- [10] CASTELLINI, P. and SCALISE, L., “Teeth mobility measurement by laser doppler vibrometer,” *Review of Scientific Instruments*, vol. 70, no. 6, pp. 2850–2855, 1999.
- [11] CASTELLINI, P., SOPRANZETTI, F., MARTARELLI, M., and TOMASINI, E. P., “Continuous Scanning LDV by Signal Re-sampling Method: A New Signal Processing Approach,” in *30th International Modal Analysis Conference (IMAC XXX) Jacksonville, Florida*, vol. 6, pp. 443–452, 2012.

- [12] CATHELINE, S., GENNISSON, J., DELON, G., FINK, M., SINKUS, R., ABOUELKARAM, S., and CULIOLI, J., “Measurement of viscoelastic properties of homogeneous soft solid using transient elastography: An inverse problem approach,” *Journal of the Acoustical Society of America*, vol. 116, pp. 3734–3741, DEC 2004.
- [13] CATHELINE, S., WU, F., and FINK, M., “A solution to diffraction biases in sonoelasticity: The acoustic impulse technique,” *Journal of the Acoustical Society of America*, vol. 105, no. 5, pp. 2941–2950, 1999.
- [14] CESCO, C., FARINA, D., GOBBO, M., MERLETTI, R., and ORIZIO, C., “Effect of accelerometer location on mechanomyogram variables during voluntary, constant-force contractions in three human muscles,” *MEDICAL & BIOLOGICAL ENGINEERING & COMPUTING*, vol. 42, pp. 121–127, JAN 2004.
- [15] DEFFIEUX, T., GENNISSON, J., TANTER, M., and FINK, M., “Assessment of the mechanical properties of the musculoskeletal system using 2-d and 3-d very high frame rate ultrasound,” *IEEE Transactions on Ultrasonic, Ferroelectrics, and Frequency Control*, vol. 55, pp. 2177 – 2190, 2008.
- [16] DRESNER, M., ROSE, G., ROSSMAN, P., MUTHUPILLAI, R., MANDUCA, A., and EHMAN, R. L., “Magnetic resonance elastography of skeletal muscle,” *Journal of Magnetic Resonance Imaging*, vol. 13, p. 269276, 2001.
- [17] DURST, F. and WHITELAW, J. H., “Optimization of optical anemometers,” *Proceedings of the Royal Society of London. Series A, Mathematical and Physical Sciences*, vol. 324, no. 1557, pp. pp. 157–181, 1971.
- [18] FUNG, Y., *Biomechanics: Mechanical Properties of Living Tissues*. New York: Springer-Verlag, 2nd ed., 1988.
- [19] GENNISSON, J.-L., DEFFIEUX, T., MACE, E., MONTALDO, G., FINK, M., and TANTER, M., “Viscoelastic and anisotropic mechanical properties of in-vivo muscle tissue assessed by supersonic shear imaging,” *Ultrasound in Medicine & Biology*, vol. 36, pp. 789–801, MAY 2010.
- [20] GENNISSON, J., CORNU, C., CATHELINE, S., FINK, M., and PORTERO, P., “Human muscle hardness assessment during incremental isometric contraction using transient elastography,” *Journal of biomechanics*, vol. 38, pp. 1543–1550, JUL 2005.
- [21] GOODE, R. L., BALL, G., and NISHIHARA, S., “Measurement of umbo vibration in human subjects—method and possible clinical applications,” *American Journal of Otology*, vol. 14, pp. 247–251, 1993.
- [22] GOODE, R. L., BALL, G., NISHIHARA, S., and K, N., “Laser doppler vibrometer (ldv)—a new clinical tool for the otologist,” *American Journal of Otology*, vol. 17, pp. 813–822, 1996.
- [23] GREENLEAF, J., FATEMI, M., and INSANA, M., “Selected methods for imaging elastic properties of biological tissues,” *Annual Review of Biomedical Engineering*, vol. 5, pp. 57–78, 2003.

- [24] HALLIWELL, N. A., PICKERING, C. J. D., and EASTWOOD, P. G., “The laser torsional vibrometer: A new instrument,” *Journal of Sound and Vibration*, vol. 93, no. 4, pp. 588–592, 1984.
- [25] HALLIWELL, N., “The laser torsional vibrometer: A step forward in rotating machinery diagnostics,” *Journal of Sound and Vibration*, vol. 190, pp. 399–418, FEB 29 1996.
- [26] HEIN, A., “Processing of SAR Data: Fundamentals, Signal Processing, Interferometry,” *Springer*, vol. 1st ed., pp. 38–44, 2004.
- [27] HOYT, K., T., K., CASTANEDA, B., , and PARKER, J., “Quantitative sonoelastography for the in vivo assessment of skeletal muscle viscoelasticity,” *Physics in Medicine & Biology*, vol. 53, pp. 4063–4080, 2008.
- [28] KENDALL, F. P., MCCREARY, E. K., PROVANCE, P. G., RODGERS, M. M., and RODGERS, M. M., *Muscles: Testing and Function, with Posture and Pain*. Lippincott Williams & Wilkins, 2005.
- [29] KLAUDER, J. R., PRICE, A. C., DARLINGTON, S., and ALBERSHEIM, W. J., “The theory and design of chirp radars,” *Bell System Technical Journal*, vol. 39, p. 745, 1960.
- [30] LA, J. P., CHOI, J., WANG, S. Y., KIM, K., and PARK, K., “Continuous scanning laser Doppler vibrometer for mode shape analysis,” *Optical Engineering*, vol. 42, no. 3, pp. 730–737, 2003.
- [31] LANDAU, L. D. and LIFSHITZ, E. M., “Theory of elasticity, third edition: (course of theoretical physics),” *Butterworth-Heinemann*, vol. 7, 1986.
- [32] LEVINSON, S., SHINAGAWA, M., and SATO, T., “Sonoelastic determination of human skeletal muscle elasticity,” *Journal of Biomechanics*, vol. 28, p. 11451154., 1995.
- [33] LEVINSON, S., SHINAGAWA, M., and SATO, T., “Sonoelastic determination of human skeletal-muscle elasticity,” *Journal of Biomechanics*, vol. 28, pp. 1145–1154, 10 1995.
- [34] MARTARELLI, M. and EWINS, D. J., “Continuous scanning laser Doppler vibrometry and speckle noise occurrence,” *Mechanical Systems and Signal Processing*, vol. 20, no. 8, pp. 2277–2289, 2006.
- [35] MARTARELLI, M., “Exploiting the laser scanning facility for vibration measurements,” *Ph.D. thesis, Imperial College London*, pp. 92–106, 2001.
- [36] MARTIN, P. and ROTHBERG, S., “Laser vibrometry and the secret life of speckle patterns,” in *Optical Sensors, Devices, and Systems II* (TOMASINI, E. P., ed.), vol. 7098, p. 709812, SPIE, 2008.
- [37] MILES, T., LUCAS, M., HALLIWELL, N., and ROTHBERG, S., “Torsional and bending vibration measurement on rotors using laser technology,” *Journal of Sound and Vibration*, vol. 226, pp. 441–467, SEP 23 1999.
- [38] MORRISON, S., KAVANAGH, J., OBST, S., IRWIN, J., and HASELER, L., “The effects of unilateral muscle fatigue on bilateral physiological tremor,” *International Journal of Biological Sciences*, vol. 167, pp. 609–621, 2005.

- [39] MUTHUPILLAI, R., LOMAS, D., ROSSMAN, P., GREENLEAF, J., MANDUCA, A., and EHMAN, R., “Magnetic resonance elastography by direct visualization of propagation acoustic strain waves,” *Science*, vol. 269, pp. 1854–1857, 1995.
- [40] ORIZIO, C., “Muscle sound - bases for the introduction of a mechanomyogram signal in muscle studies,” *Crit Rev Biomed Eng.*, vol. 21, no. 3, pp. 201–243, 1993.
- [41] PERRY, S., HOUSH, T., WEIR, J., JOHNSON, G., BULL, A., and EBERSOLE, K., “Mean power frequency and amplitude of the mechanomyographic and electromyographic signals during incremental cycle ergometry,” *Journal of Electromyography and Kinesiology*, vol. 11, pp. 299–305, AUG 2001.
- [42] RATILAL, P., ANDREWS, M., DONABED, N., GALINDE, A., RAPPAPORT, C., and FENNEMAN, D., “Model for continuously scanning ultrasound vibrometer sensing displacements of randomly rough vibrating surfaces,” *Journal of the Acoustical Society of America*, vol. 121, pp. 863–878, FEB 2007.
- [43] RINGLEB, S., BENSAMOUN, S., CHEN, Q., MANDUCA, A., AN, K., and EHMAN, R., “Applications of magnetic resonance elastography to healthy and pathologic skeletal muscle,” *Journal of Magnetic Resonance Imaging*, vol. 25, pp. 301–309, 2007.
- [44] ROBLES-DE-LA-TORRE, G., “Principles of haptic perception in virtual environments,” *Human haptic perception*, pp. 363–379, 2008.
- [45] ROSSI, G. L. and TOMASINI, E. P., “Proposal of a new measurement technique for hand-arm vibration analysis,” in *First International Conference on Vibration Measurements by Laser Techniques: Advances and Applications* (TOMASINI, E. P., ed.), vol. 2358, pp. 48–59, Proc. SPIE, 1994.
- [46] ROTHBERG, S., “Laser vibrometry pseudo-vibrations,” *Journal of Sound and Vibration*, vol. 135, no. 3, pp. 516–522, 1989.
- [47] RUZZENE, M., “Frequency-wavenumber domain filtering for improved damage visualization,” *Smart Materials & Structures*, vol. 16, pp. 2116–2129, DEC 2007.
- [48] SABRA, K. G., CONTI, S., ROUX, P., and KUPERMAN, W. A., “Passive in vivo elastography from skeletal muscle noise,” *Applied Physics Letters*, vol. 90, pp. 194101, L07–01965R, MAY 7 2007.
- [49] SABRA, K. and ARCHER, A., “Tomographic elastography imaging of skeletal muscles from their natural vibrations,” *Applied Physics Letters*, vol. 95, p. L 203701, 2009.
- [50] SALE, D. G. and KOMI, P., *Neural Adaptation to Strength Training*, vol. 3, ch. Strength and Power in Sport, p. 544. Wiley-Blackwell Science Ltd, 2nd ed., 2008.
- [51] SALTER, R., *Textbook of disorders and injuries of the musculoskeletal system: An introduction to orthopaedics, fractures, and joint injuries, rheumatology, metabolic bone disease, and rehabilitation*. Baltimore, MD: Wilkins & Wilkins, 1999.
- [52] SANDRIN, L., CATHELIN, S., TANTER, M., HENNEQUIN, X., and FINK, M., “Time-resolved pulsed elastography with ultrafast ultrasonic imaging,” *Ultrasonic Imaging*, vol. 21, pp. 259–272, 4 1999.

- [53] SANDRIN, L., TANTER, M., CATHELINE, S., and FINK, M., “Shear modulus imaging with 2-D transient elastography,” *IEEE Transactions on Ultrasonics Ferroelectrics and Frequency Control*, vol. 49, pp. 426–435, 4 2002.
- [54] SANDRIN, L., TANTER, M., GENNISSON, J., CATHELINE, S., and FINK, M., “Shear elasticity probe for soft tissues with 1-d transient elastography,” *IEEE Transactions on Ultrasonics Ferroelectrics and Frequency Control*, vol. 49, pp. 436–446, 4 2002.
- [55] SHANNON, C., “Communication in the presence of noise,” *Proceedings of the Institute of Radio Engineers*, vol. 37, pp. 10–21, 1949.
- [56] SHINOHARA, M., SABRA, K., GENNISSON, J.-L., FINK, M., and TANTER, M., “Real-time visualization of muscle stiffness distribution with ultrasound shear wave imaging during muscle contraction,” *Muscle & Nerve*, vol. 42, pp. 438–441, SEP 2010.
- [57] SMAGA, S., “Tremor,” *American Academy of Family Physicians*, vol. 68, pp. 1542–52, 2003.
- [58] SRACIC, M. W. and ALLEN, M. S., “Experimental investigation of the effect of speckle noise on continuous scan laser Doppler vibrometer measurements,” in *27th International Modal Analysis Conference (IMAC XXVII), Orlando, Florida*, 2009.
- [59] SRACIC, M. W., “A new experimental modal analysis method using continuous scan laser doppler vibrometry and impact excitation.” University of Wisconsin,, 2008. Masters Thesis.
- [60] SRIRAM, P., “Whole field optical methods for structural mechanics: Digital speckle correlation and laser doppler velocimetry,” *Ph.D. thesis, Georgia Institute of Technology*, pp. 38–41, March 1988.
- [61] SRIRAM, P., CRAIG, J., and HANAGUD, S., “Scanning laser Doppler techniques for vibration testing,” *Experimental Techniques*, vol. 16, no. 6, pp. 21–26, 1992.
- [62] SRIRAM, P., HANAGUD, S., CRAIG, J., and KOMERATH, N., “Scanning laser Doppler technique for velocity profile sensing on a moving surface,” *Applied Optics*, vol. 29, no. 16, pp. 2409–2417, 1990.
- [63] SRIRAM, P., HANAGUD, S., and CRAIG, J., “Mode shape measurement using a scanning laser Doppler vibrometer,” *The International journal of analytical and experimental modal analysis*, vol. 7, no. 3, pp. 169–178, 1992.
- [64] SRIRAM, P., HANAGUD, S. V., and CRAIG, J. I., “Scanning laser Doppler technique for modal testing of distributed-parameter systems,” *AIAA journal*, vol. 30, no. 2, pp. 765–766, 1992.
- [65] STANBRIDGE, A. B. and EWINS., D. J., “Modal testing using a scanning laser Doppler vibrometer,” *Mechanical Systems and Signal Processing*, vol. 13(2), pp. 255–270, 1999.
- [66] STANBRIDGE, A. B. and EWINS, D. J., “Measurement of translational and angular vibration using a scanning laser Doppler vibrometer,” in *SPIE* (TOMASINI, E. P., ed.), vol. 2358, pp. 37–47, 1994.

- [67] STANBRIDGE, A. B., MARTARELLI, M., and EWINS, D. J., “Measuring area vibration mode shapes with a continuous-scan LDV,” *Measurement*, vol. 35, pp. 181–189, March 2004.
- [68] TAKAI, N. and ASAKURA, T., “Dynamic statistical properties of vibrating laser speckle in diffraction field,” *Applied Optics*, vol. 17, no. 23, pp. 3785–3793, 1978.
- [69] TURIN, G. L., “An introduction to matched filters,” *IRE Transactions on Information Theory*, vol. 6, pp. 311–329, June 1960.
- [70] URBAN, M., CHEN, S., and GREENLEAF, J., “Error in estimates of tissue material properties from shear wave dispersion ultrasound vibrometry,” *IEEE Transactions on Ultrasonics Ferroelectrics and Frequency Control*, vol. 56, pp. 748–758, 2009.
- [71] VANLANDUIT, S., GUILLAUME, P., and SCHOUKENS, J., “Broadband vibration measurements using a continuously scanning laser vibrometer,” *Measurement Science and Technology, Institute of Physics Publishing*, vol. 13, pp. 1574–1582, 2002.
- [72] WILSON, G., MURPHY, A., and PRYOR, J., “Musculotendinous Stiffness - Its Relationship to Eccentric, Isometric, and Concentric Performance,” *Journal of Applied Physiology*, vol. 7, pp. 2714–2719, 1994.
- [73] WINTER, D. A., *Biomechanics and Motor Control of Human Movement*. John Wiley & Sons, 2004.
- [74] YANG, S. and ALLEN, M. S., “Output-only modal analysis using continuous-scan laser Doppler vibrometry and application to a 20kW wind turbine,” in *29th International Modal Analysis Conference (IMAC XXIX) Jacksonville, Florida*, vol. 3, pp. 47–64, 2011.
- [75] YEH, Y. and CUMMINS, H., “Localized fluid flow measurements with he-ne laser spectrometer,” *Applied Physics Letters*, vol. 4, no. 10, pp. 176 – 178, 1964.
- [76] YUCESOY, C. and P.A., H., “Substantial effects of epimuscular myofascial force transmission on muscular mechanics have major implications on spastic muscle and remedial surgery,” *Journal of Electromyography and Kinesiology*, vol. 17, p. 664679, 2007.
- [77] ZHENG, Y., MAK, A., and LUE, B., “Objective assessment of limb tissue elasticity: Development of a manual indentation procedure,” *Journal of Rehabilitation Research and Development*, vol. 36, pp. 71–85, 2 1999.